Article

Cell Stem Cell

RAL GTPases Drive Intestinal Stem Cell Function and Regeneration through Internalization of WNT Signalosomes

Graphical Abstract

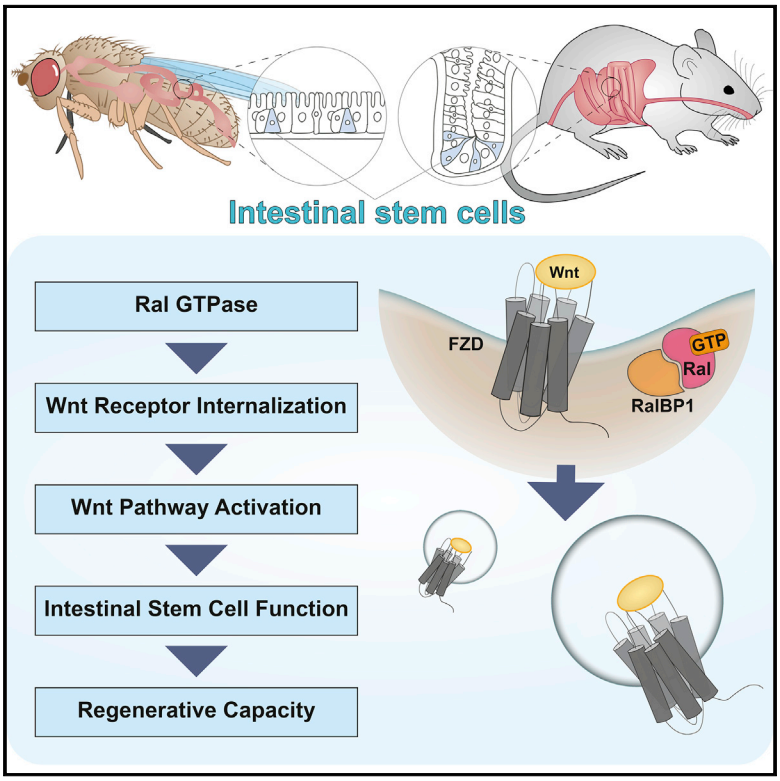

Authors

Joel Johansson, Mate Naszai, Michael C. Hodder, ..., Andrew D. Campbell, Julia B. Cordero, Owen J. Sansom

Correspondence

julia.cordero@glasgow.ac.uk (J.B.C.), o.sansom@beatson.gla.ac.uk (O.J.S.)

In Brief

RAL GTPases are central players in intestinal biology. RALs are required to activate canonical Wnt signaling in *Drosophila*, mice, and human cell lines. Within intestinal stem cells, RALs are essential to sustain tissue homeostasis and regeneration. RAL small GTPases modulate Wnt pathway activity through internalization of cell-surface Wnt receptors.

Highlights

- RAL GTPases are widely expressed in the intestinal epithelium
- RAL GTPases activate Wnt signaling through internalization of Wnt receptors
- RAL GTPase signaling is required for optimal stem cell numbers
- RAL GTPases drive regeneration of fruit fly and mouse intestine following damage

Johansson et al., 2019, Cell Stem Cell *24*, 592–607
April 4, 2019
https://doi.org/10.1016/j.stem.2019.02.002

CellPress

CellPress

Cell Stem Cell
Article

RAL GTPases Drive Intestinal Stem Cell Function and Regeneration through Internalization of WNT Signalosomes

Joel Johansson,[1,5] Mate Naszai,[2,5] Michael C. Hodder,[1] Karen A. Pickering,[1] Bryan W. Miller,[1] Rachel A. Ridgway,[1] Yachuan Yu,[1,2] Pascal Peschard,[3] Saskia Brachmann,[4] Andrew D. Campbell,[1] Julia B. Cordero,[2,*] and Owen J. Sansom[1,2,6,*]

[1]Cancer Research UK Beatson Institute, Glasgow G61 1BD, UK
[2]Institute of Cancer Sciences, University of Glasgow, Glasgow G61 1QH, UK
[3]McGill University, Montréal, Quebec, Canada
[4]Novartis Institutes for Biomedical Research, Basel, Switzerland
[5]These authors contributed equally
[6]Lead Contact
*Correspondence: julia.cordero@glasgow.ac.uk (J.B.C.), o.sansom@beatson.gla.ac.uk (O.J.S.)
https://doi.org/10.1016/j.stem.2019.02.002

SUMMARY

Ral GTPases are RAS effector molecules and by implication a potential therapeutic target for RAS mutant cancer. However, very little is known about their roles in stem cells and tissue homeostasis. Using *Drosophila*, we identified expression of RalA in intestinal stem cells (ISCs) and progenitor cells of the fly midgut. RalA was required within ISCs for efficient regeneration downstream of Wnt signaling. Within the murine intestine, genetic deletion of either mammalian ortholog, *Rala* or *Ralb*, reduced ISC function and Lgr5 positivity, drove hypersensitivity to Wnt inhibition, and impaired tissue regeneration following damage. Ablation of both genes resulted in rapid crypt death. Mechanistically, RALA and RALB were required for efficient internalization of the Wnt receptor Frizzled-7. Together, we identify a conserved role for RAL GTPases in the promotion of optimal Wnt signaling, which defines ISC number and regenerative potential.

INTRODUCTION

RAL GTPases (RALs) are RAS effectors critical for tumor initiation (Lim et al., 2005) and anchorage independent growth of colorectal cancer (CRC) cell lines (Martin et al., 2011). Consequently, RALs are potential therapeutic targets in this setting (Neel et al., 2011; Yan et al., 2014). The mammalian genome encodes for two RALs, RALA and RALB, with non-redundant functions spanning development (Peschard et al., 2012), exocyst formation (Bodemann and White, 2008; Chen et al., 2007; Chien et al., 2006), and endocytosis. Specifically, the RAL effector RALBP1 drives clathrin-mediated endocytosis (Jullien-Flores et al., 2000), while RALA promotes caveolar endocytosis (Jiang et al., 2016). RAL activity is potentiated by RAL guanine nucleotide exchange factors (RALGEFs) and negatively regulated by RAL GTPase-activating proteins (RALGAPs) (Neel et al., 2011). Multiple RALGEF molecules, such as RALGDS, contain RAS-binding domains and are activated by association with oncogenic RAS (Koyama and Kikuchi, 2001). Indeed, RALGDS has a reported role in tumor initiation and growth (González-García et al., 2005; Rodriguez-Viciana and McCormick, 2005). However, the precise role of RALs or associated effectors in intestinal biology remains unknown.

Wnt signaling is critical in intestinal health and disease. Impaired signaling leads to crypt death (Ireland et al., 2004; Kuhnert et al., 2004), while pathway hyperactivation drives cancer (Clevers, 2006). Balanced pathway activity is essential to maintain tissue homeostasis while preventing tumorigenesis. High Wnt signaling is found at the crypt base (Gregorieff et al., 2005), where intestinal stem cells (ISCs) and Paneth cells exhibit nuclear β-catenin and transcriptional signatures associated with Wnt pathway activation. A subset of ISCs also express Lgr5, which potentiates Wnt signaling by binding to the agonist R-Spondin (R-Spo) (Barker et al., 2007; Sato et al., 2009). $Lgr5^{+}$ ISCs are redundant for homeostasis but required for regeneration following damage (Metcalfe et al., 2014). Wnt ligands are expressed in numerous cell lineages within the intestinal epithelium and its microenvironment, including Paneth and mesenchymal cells (Shoshkes-Carmel et al., 2018; Valenta et al., 2016; Zou et al., 2018). Removal of Paneth cell-derived Wnt affects outgrowth of crypts as organoids, whereas the mesenchymal source is enough to sustain crypts *in vivo* (Degirmenci et al., 2018; Kim et al., 2012; Sato et al., 2011; Shoshkes-Carmel et al., 2018). The redundant Wnt stem cell niche is conserved in the *Drosophila melanogaster* intestine. *Drosophila* Wnt/Wg produced by uncommitted progenitor cells called enteroblasts (EBs) is specifically required for ISC proliferation upon stress and regeneration, while the mesenchyme-derived ligand is sufficient to maintain tissue homeostasis (Cordero et al., 2012b; Lin et al., 2008).

The Wnt signalosome is composed of a cluster of Frizzled receptors, Lrp5/6 co-receptors, and Dishevelled (Dvl) at the plasma membrane (Bilic et al., 2007; Chung et al., 2012;

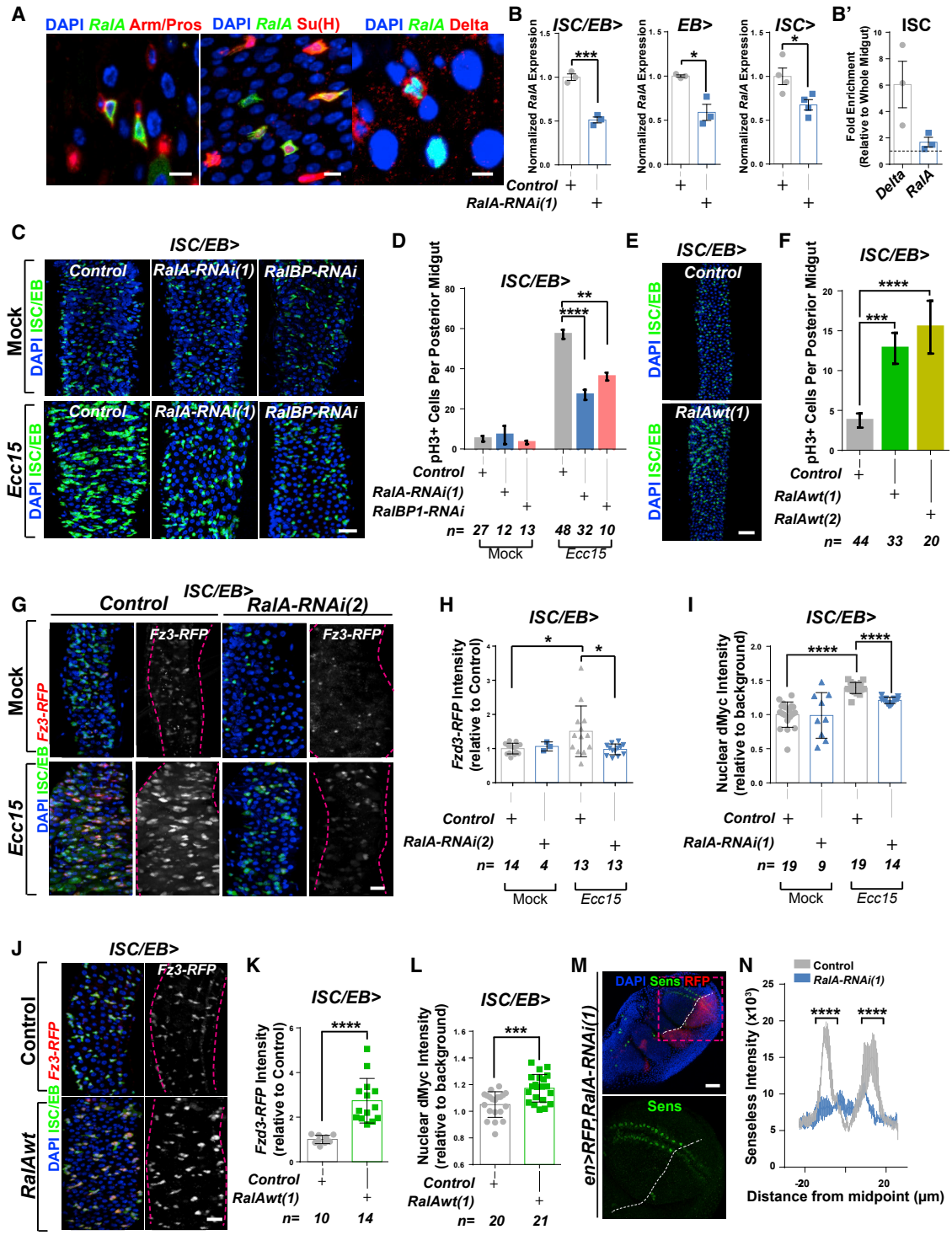

Figure 1. Ral Small GTPase Signaling Controls the Regenerative Capacity of the *Drosophila* Midgut through Wnt Signaling

(A) Co-labeling of *RalA>GFP* (green) with markers for ISCs/EBs (Arm; red membrane staining), EEs (Pros; red nuclear staining), EBs (*Su(H)GBE-LacZ*; red); RalA > nRFP (green pseudo colored), or ISCs (*Delta::GFP*; red). Scale bar, 5 μm.

(B) *RalA* transcript levels relative to *rpl32* in whole midgut samples following indicated cell-type-specific *RalA* knockdown (*RalA-RNAi(1)*) normalized to 1. Student's t test; ISC/EB, EB n = 3, ISC n = 4; error bars, ± SEM.

(B′) *RalA* transcript levels in sorted ISCs relative to whole midgut samples. *Delta* is used to confirm ISC enrichment. n = 3; error bars, ± SEM.

(C) Representative confocal images of mock-treated or regenerating (*Ecc15*) adult posterior midguts from control animals or upon adult-specific *RalA* or *RalBP* knockdown by RNAi (*RalA-RNAi(1)* and *RalBP-RNAi*, respectively) within stem and progenitor cells (ISCs/EBs; green) using the *escargot-gal4, UAS-gfp* driver. Scale bar, 20 μm.

(legend continued on next page)

Schwarz-Romond et al., 2007). An important step in the assembly of the Wnt signalosome involves polymerization of Dvl and interaction with Frizzled receptors during ligand-induced endocytosis of the receptor complex (Gammons et al., 2016). Once assembled, the Wnt signalosome immobilizes the β-catenin destruction complex and stabilizes β-catenin, activating transcription of Wnt target genes (Kishida et al., 1999; MacDonald et al., 2009). Altogether, evidence suggests that the regulation of Wnt activity through ligand availability and cell-surface receptor internalization is critical in control of ISC proliferation and differentiation states.

Here, we used *Drosophila* and mouse models to address the biological function of RALs in the adult intestine. Our results demonstrate a conserved *in vivo* role for RALs in ISC function during tissue homeostasis and regeneration. ISCs lacking RALs were at a disadvantage compared to wild-type neighbors. Importantly, we show that constitutive β-catenin activation through *APC* deletion rescued the suppression of Wnt signaling following RAL loss, and that RALs promote Wnt signaling through control of Wnt signalosome internalization.

RESULTS

RalA Is Required for Intestinal Regeneration and Wnt Signaling Activation in *Drosophila*

The epithelium of the adult *Drosophila* midgut, homologous to the mammalian small intestine (SI) (Casali and Batlle, 2009; Lemaitre and Miguel-Aliaga, 2013), consists of ISCs, undifferentiated progenitors called EBs, secretory enteroendocrine cells (EEs), and absorptive enterocytes (ECs). ISCs proliferate to self-renew the midgut epithelium in homeostatic conditions as well as to drive tissue regeneration following damage by pathogenic bacteria or other toxic stimuli, through activation of conserved signaling pathways (Micchelli and Perrimon, 2006; Nászai et al., 2015; Ohlstein and Spradling, 2006).

Expression of the single *Ral GTPase* fly ortholog, *RalA*, appears enriched in the adult *Drosophila* midgut (http://flyatlas.org/atlas.cgi). A *gal4* insertion within the endogenous gene locus (*RalA-gal4*) (Bourbon et al., 2002) in combination with a *gal4*-responsive *UAS-GFP* transgene (*RalA>GFP*) confirmed *RalA* expression throughout the adult fly midgut and in enteric neuronal projections (Figure S1A). Co-labeling experiments in the posterior midgut epithelium showed *RalA* expression in ISCs/EBs, marked by Armadillo (Arm), but not in EEs, labeled with nuclear Prospero (Pros) (Figure 1A). Combining the EB-specific transgenic reporter *Su(H)GBE-LacZ* with *RalA>GFP* and an endogenous GFP-tagged form of the ISC marker Delta with *RalA > nRFP* showed *RalA* co-labeling with ISCs and EBs (Figure 1A). Consistently, reverse transcription quantitative polymerase chain reaction (RT-qPCR) revealed significant reduction of *RalA* transcript levels in whole midguts following targeted *RalA* knockdown by RNA interference (*RalA-RNAi(1)*) in ISCs and EBs or individually in each cell population (Figure 1B). RT-qPCR confirmed *RalA* expression in sorted ISCs (Figure 1B′). However, *RalA* is not enriched in ISCs (Figure 1B′), which can be partly explained by reporter expression in the visceral muscle (VM) (Figure S1A) and correlates with data from *Flygut-seq* (http://flygutseq.buchonlab.com).

To assess the role of *RalA* in homeostatic ISC self-renewal, we performed lineage tracing experiments from control and *RalA-RNAi*-expressing ISCs using two independent GFP^{+ve} ISC lineage tracing systems. The "*escargot flip out*" (*ISC/EB Flipout*) system (Jiang et al., 2009), resulting in transgene expression and lineage tracing of every ISC/EB (Figures S1B and S1C), and the MARCM system, which generates clones following Flipase (FLP)/FRT, mediated mitotic recombination, leading to transgene expression and labeling of a discrete subset of ISCs (Lee and Luo, 2001) (Figures S1D and S1E). Results from both lineage tracing systems showed no difference in the size of control and *RalA-RNAi*-expressing clones (Figures S1B–S1E). MARCM clones also revealed no change in ISC lineage differentiation following *RalA* knockdown (Figures S1F and S1G).

We next assessed whether RalA was required to drive the proliferative response of ISCs following intestinal epithelial damage

(D) Quantification of $pH3^+$ cells in posterior midguts as in (C). Two-way ANOVA is shown, followed by Sidak's multiple comparisons test; n = number of posterior midguts quantified; error bars, ± SEM.
(E) Representative confocal images of control or wild-type *RalA* ISC/EB-overexpressing posterior midguts (*RalAwt(1)*) (ISC/EB; green). Scale bar, 50 μm.
(F) Quantification of $pH3^+$ cells in posterior midguts overexpressing independent *RalA* constructs (*RalAwt(1)* and *RalAwt(2)*). One-way ANOVA is shown, followed by Sidak's multiple comparisons test; n = number of posterior midguts quantified; error bars, ± SEM.
(G) Representative confocal images of Wnt pathway activity reporter *Fz3-RFP* (red or gray) in mock-treated or regenerating (*Ecc15*) adult posterior midguts from control animals or animals subject to adult-specific RalA knockdown (*RalA-RNAi(2)*) within ISCs/EBs. Scale bar, 20 μm.
(H) Quantification of the average *Fz3-RFP* staining intensity within the ISC/EB compartment in posterior midguts as in (G), normalized to 1. Two-way ANOVA is shown, followed by Sidak's multiple comparisons test; each dot represents values from a z stack confocal image from a posterior midgut; error bars, ± SD.
(I) Quantification of the average nuclear dMyc staining intensity within the ISC/EB compartment in mock-treated or regenerating (*Ecc15*) posterior midguts of control or *RalA* knockdown (*RalA-RNAi(1)*) normalized to background staining. Two-way ANOVA is shown, followed by Sidak's multiple comparisons test; each dot represents values from a z stack confocal image from a posterior midgut; error bars, ± SD.
(J) Representative confocal images of Wnt pathway activity reporter *Fz3-RFP* (red or gray) from control animals or animals overexpressing wild-type *RalA* in ISCs/EBs. Scale bar, 20 μm.
(K) Quantification of the average *Fz3-RFP* staining in posterior midguts as in (J), normalized to 1. Student's t test is shown; each dot represents a z stack confocal image from a posterior midgut; error bars, ± SD.
(L) Quantification of the average nuclear dMyc staining intensity within the ISC/EB compartment in control or *RalA*-overexpressing midguts normalized to background staining. Student's t test is shown; each dot represents values from z stack confocal image from a posterior midgut; error bars, ± SD.
(M) Representative confocal images of Senseless staining (Sens; green) in third-instar larval wing discs upon *RalA* knockdown (*RalA-RNAi(1)*) in the posterior compartment (RFP positive) using the *engrailed>RFP* driver. Scale bar, 50 μm.
(N) Quantification of Senseless staining intensity perpendicular to the line Senseless expression in the control (RFP negative) versus the *RalA* knockdown (RFP positive) compartment in larval wing discs. Multiple t tests, false discovery rate [FDR] = 0.01; n = 4 wing discs; error bars, ± SEM.
Where indicated, *p < 0.05, **p < 0.01, ***p < 0.001, ****p < 0.0001.

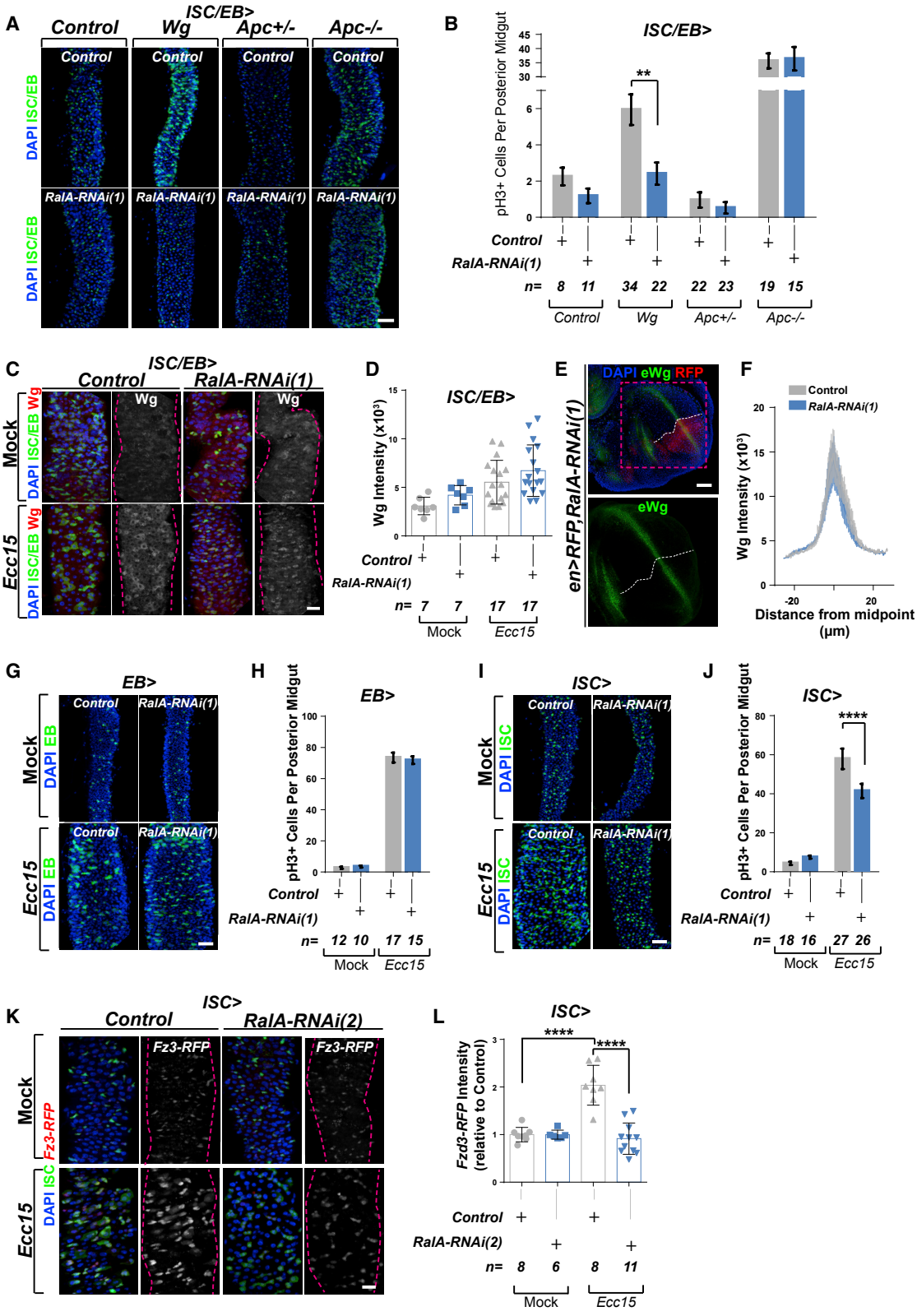

Figure 2. *Drosophila* Ral Is Required in ISCs for Wnt Signaling Activation, Upstream of the β-Catenin Destruction Complex

(A) Representative confocal images of control, Wg-overexpressing, *Apc* heterozygous ($Apc^{+/-}$), and *Apc* mutant ($Apc^{-/-}$) posterior midguts with or without *RalA* knockdown (*RalA-RNAi(1)*) in ISCs/EBs. Scale bar, 50 μm.

(legend continued on next page)

by oral bacterial infection with the pathogen *Erwinia carotovora carotovora* (*Ecc15*) (Basset et al., 2000). We quantified ISC proliferation through scoring of pH3 positive cells in posterior midguts from control animals and animals following *RalA-RNAi* expression within ISCs/EBs using the *escargot-gal4* driver (Micchelli and Perrimon, 2006; Figures 1C and 1D). We observed approximately 50% decrease in damage-induced ISC proliferation in *RalA* knockdown animals (Figure 1D). This phenotype was recapitulated with two additional, independent *RalA-RNAi*s (Figure S2A) and upon knockdown of the RAL GTPase effector *RalBP1* (Figures 1C and 1D). These results show that RNAi-mediated knockdown of *RalA* does not alter gut homeostasis in *Drosophila* but impairs ISC proliferation during damage-induced regeneration of the intestine. Reciprocally, overexpression of *RalA* in ISCs/EBs using two independent constructs was sufficient to induce ISC proliferation in the posterior midgut (Figures 1E and 1F).

Inducible Wnt ligand (Wingless; Wg) secretion from progenitor cells (EBs) is required for intestinal regeneration in *Drosophila* but is dispensable for steady-state tissue maintenance (Cordero et al., 2012b). We therefore hypothesized that the damage-specific role of *RalA* in the intestine might be mediated through regulation of Wnt signaling. To investigate this further, we combined *RalA* knockdown with a transgenic reporter of Wnt signaling (*Fz3-RFP*) (Olson et al., 2011). Control animals showed *Fz3-RFP* significantly upregulated within ISCs/EBs of the posterior midgut following damage, while *RalA* knockdown impaired *Fz3-RFP* upregulation in damaged tissues (Figures 1G and 1H). A similar result was observed for dMyc, which is a known target of Wnt signaling during regeneration and aging (Cordero et al., 2012a; Figures 1I and S2B). Consistent with our gain-of-function data (Figures 1E and 1F), overexpression of *RalA* within ISC/EBs was sufficient to induce upregulation of *Fz3-RFP* and dMyc expression (Figures 1J–1L and S2C). Importantly, the role of *RalA* on Wnt signaling was not restricted to the midgut, as evidenced by downregulation of the Wnt signaling target Senseless in the larval wing disc, following domain-specific *RalA* knockdown (Figures 1M, 1N, and S2F–S2H). Together, these data suggest that RalA is necessary and sufficient for Wnt signaling activation *in vivo*.

RalA Regulates Wnt Signaling Upstream of the β-Catenin Destruction Complex in *Drosophila* ISCs

We next assessed how Wnt signaling pathway is regulated by *RalA* in the *Drosophila* gut. Ectopic activation of the Wnt pathway through overexpression of Wg or following deletion of *Apc* drives ISC hyperproliferation (Cordero et al., 2012b; Figures 2A and 2B). Remarkably, only ISC proliferation induced by overexpression of Wg was suppressed by concomitant *RalA* knockdown (Figures 2A, 2B, S2D, and S2E). This suggests the role of RalA on Wnt signaling lies upstream of the β-catenin destruction complex and downstream of the Wg ligand.

We next investigated whether *RalA* knockdown impaired production or secretion of Wnt ligands. Critically, knockdown of *RalA* did not affect damage-induced Wg production (Figures 2C and 2D; Cordero et al., 2012b). Similarly, *RalA* status had no impact upon levels of extracellular Wg (eWg) in the larval *Drosophila* wing disc (Figures 2E, 2F, and S2I–S2K; Strigini and Cohen, 2000). These data suggest that RalA functions within cells receiving the signal from the Wg ligand. In response to damage, Wg mainly secreted by EBs activates Wg signaling within ISCs (Cordero et al., 2012b). Consistently, *RalA* knockdown in EBs alone had no effect on fly midgut regeneration (Figures 2G, 2H, and S2L), while *RalA* knockdown in ISCs only significantly impaired midgut regeneration using two independent RNAi constructs (Figures 2I, 2J, and S2M). These results suggest a cell-autonomous role for RalA regulating Wnt signaling activation within ISCs during regeneration. Accordingly, *RalA* knockdown in ISCs but not EBs impaired *Fz3-RFP* and dMyc upregulation upon damage (Figures 2K, 2L, and S2N–S2Q).

Taken together, these results strongly suggest that *RalA* has a stem cell-autonomous role in controlling of Wnt signaling activation upstream of the β-catenin destruction complex in the adult fly midgut.

(B) Quantification of $pH3^+$ cells in posterior midguts as in (A). Two-way ANOVA is shown, followed by Sidak's multiple comparisons test; n = number of posterior midguts quantified; error bars, ± SEM.

(C) Representative confocal images of Wg staining intensity (red or gray) within the ISC/EB compartment in mock-treated or regenerating (*Ecc15*) control or *RalA* knockdown (*RalA-RNAi(1)*) posterior midguts. Scale bar, 20 μm.

(D) Quantification of the average Wg staining intensity within the ISC/EB compartment in posterior midguts as in (C). Two-way ANOVA is shown, followed by Sidak's multiple comparisons test; each dot represents values from z stack confocal image from a posterior midgut; error bars, ± SD.

(E) Representative confocal images of extracellular Wg staining (eWg; green) in imaginal discs upon *RalA* knockdown (*RalA-RNAi(1)*) in the posterior compartment (RFP positive) using the *engrailed>RFP* driver. Scale bar, 50 μm.

(F) Quantification of extracellular Wg staining intensity perpendicular to the line of Wg secretion in control (RFP negative) versus *RalA* knocked down (RFP positive) larval wing discs. Multiple t tests, FDR = 0.01; n = 4 wing discs; error bars, ± SEM.

(G) Representative confocal images of mock-treated and regenerating (*Ecc15*) adult posterior midguts from control animals or animals subject to adult-specific *RalA* knockdown within EBs (green) using the *Su(H)GBE-gal4*, *UAS-gfp* driver. Scale bar, 50 μm.

(H) Quantification of $pH3^+$ cells posterior midguts as in (G). Two-way ANOVA is shown, followed by Sidak's multiple comparisons test; n = number of posterior midguts quantified; error bars, ± SEM.

(I) Representative confocal images of mock-treated and regenerating (*Ecc15*) adult posterior midguts from control animals or animals subject to adult-specific *RalA* knockdown within ISCs (green) using the *esg-gal4;Su(H)GBE-gal80* driver. scale bar, 50 μm)

(J) Quantification of $pH3^+$ cells in posterior midguts as in (I). Two-way ANOVA is shown, followed by Sidak's multiple comparisons test; n = number of posterior midguts quantified; error bars, ± SEM.

(K) Representative confocal images of the Wnt pathway activity reporter *Fz3-RFP* (red or gray) in mock-treated or regenerating (*Ecc15*) adult posterior midguts from control animals or animals subject to adult-specific *RalA* knockdown (*RalA-RNAi(2)*) within ISCs (green). Scale bar, 20 μm.

(L) Quantification of the average *Fz3-RFP* staining intensity within the ISC compartment in posterior midguts as in (K), normalized to 1. Two-way ANOVA is shown, followed by Sidak's multiple comparisons test; each dot represents a z stack confocal image from a posterior midgut; error bars, ± SD.

Where indicated, $^{**}p < 0.01$ $^{****}p < 0.0001$.

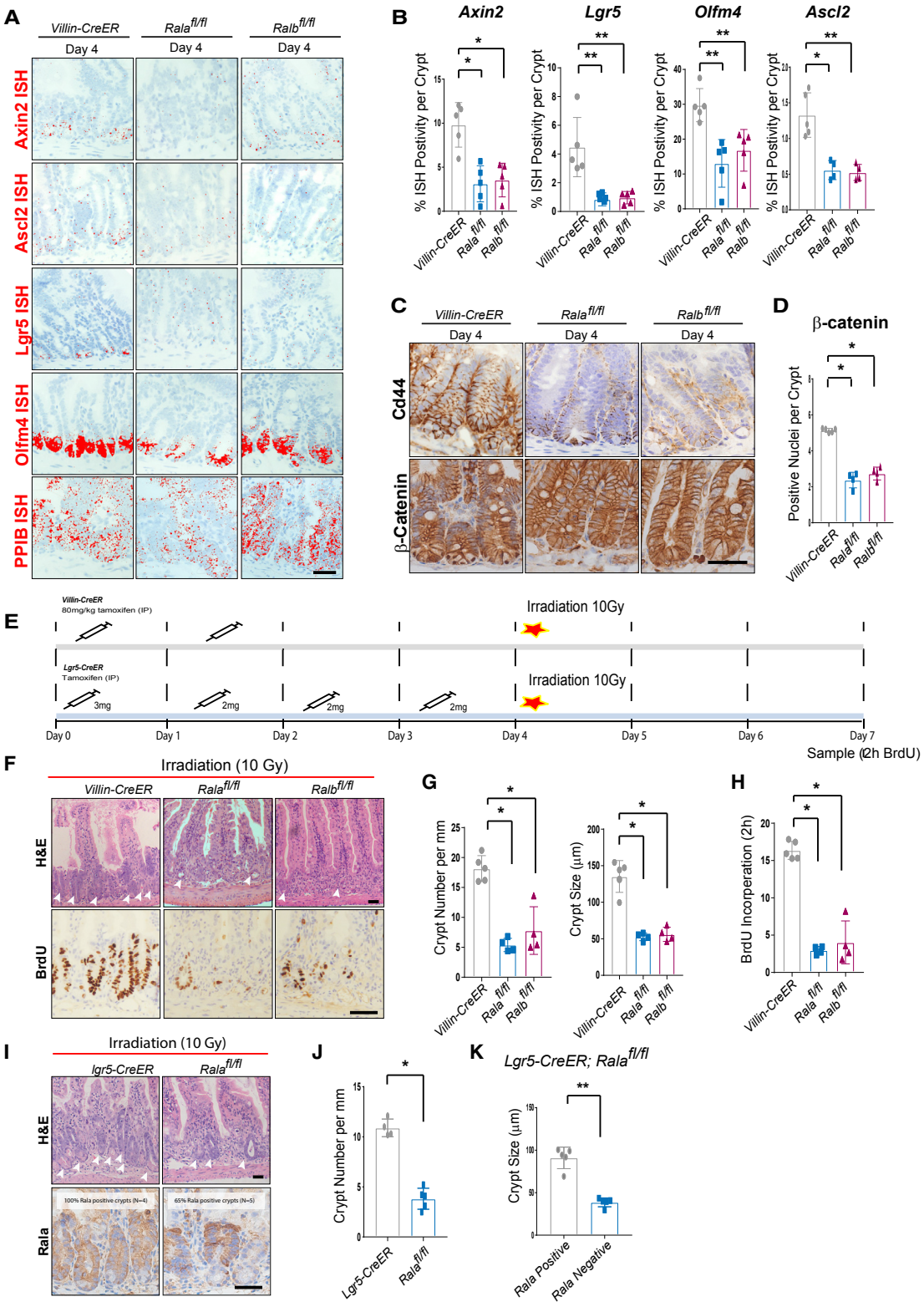

Figure 3. Loss of Either RALA or RALB Suppresses Wnt Signaling in the Murine Intestine

(A) Representative *in situ* hybridization (ISH) images of Wnt target gene expression; *Axin2*, *Ascl2*, *Lgr5*, and *Olfm4* in the small intestine after *Rala* and *Ralb* deletion (red). *Ppib* used as positive control. Scale bar, 50 μm.

(B) Quantification of ISH staining in 25 crypts per mouse, WT = 5, $Rala^{fl/fl}$ = 5, $Ralb^{fl/fl}$ = 4 or 5 for *Axin2*, *Lgr5*, *Olfm4*, and *Ascl2*. Error bars, ± SD.

(legend continued on next page)

Loss of RALA or RALB Suppresses Wnt Signaling in the Murine Intestine

Given the impact of *RalA* deletion in *Drosophila*, we predicted that loss of *Rala* or *Ralb* would reduce Wnt signaling in the murine intestine. As both isoforms are expressed within the intestinal crypt, we generated intestinal-specific conditional knockout mice for *Rala* or *Ralb* to test this hypothesis (Figure S3A). Genetic deletion of *Rala* was confirmed by immunohistochemistry (IHC) for RALA and transcriptionally by qPCR (Figures S3B and S3D), and for *Ralb* through both qPCR and RNA *in situ* hybridization (RNA-ISH) targeting the deleted exon (Figures S3C and S3D). *VillinCreER* $Rala^{fl/fl}$ and *VillinCreER* $Ralb^{fl/fl}$ intestines were examined 4 days post-induction (PI) of recombination and exhibited no significant alterations in gross intestinal morphology or epithelial proliferation (Figures S3E and S3F). Moreover, analysis of periodic acid-Schiff (PAS) or Alcian blue stains and IHC for LYSOZYME indicated that goblet and Paneth cell lineages, respectively, were also unaffected (Figure S3G). These observations suggest *Rala* and *Ralb* have redundant functions in mammalian intestinal homeostasis.

While the intestinal epithelium was viable following deletion of *Rala* or *Ralb*, this did not preclude alterations in ISC number or Wnt pathway activation. It is known that inhibition rather than ablation of Wnt signaling can reduce expression of Wnt target genes and ISC markers, rather than perturb intestinal homeostasis (Flanagan et al., 2015; Huels et al., 2018; Metcalfe et al., 2014; Yan et al., 2017). To gain a spatial overview of RNA expression of Wnt regulated genes in the SI, we performed RNA *in situ* hybridization (RNAscope). This indicated reduced expression of the canonical Wnt target genes *Axin2* and *Ascl2* in the intestinal crypts of $Rala^{fl/fl}$ and $Ralb^{fl/fl}$ mice. Similarly, the ISC markers *Lgr5* and *Olfm4* were decreased following deletion of either isoform (Figures 3A and 3B), as were the number of intestinal crypt cells expressing these markers (Figure S3H). This was confirmed by reduced expression of the stem cell marker CD44 following *Rala* or *Ralb* deletion (Figure 2C). To directly assess Wnt pathway activation, we scored for nuclear β-catenin, finding significantly fewer positive nuclei in the intestinal crypts of $Rala^{fl/fl}$ and $Ralb^{fl/fl}$ mice (Figures 3C and 3D). These data indicate that, as with *RalA* in *Drosophila*, loss of *Rala* or *Ralb* reduces Wnt signaling in the murine intestinal epithelium. As maintenance of the $Lgr5^{+}$ ISC pool requires high levels of Wnt signaling, this is consistent with a marked reduction in the size of this population.

Since intestinal regeneration following damage is Wnt ligand dependent (Ashton et al., 2010; Saha et al., 2016), and, considering *RalA* activity in the fly intestine, we sought to determine the impact of *Rala* or *Ralb* deletion upon intestinal regeneration (Figure 3E). Exposure of mice in which intestinal *Rala* or *Ralb* had been deleted (*VillinCreER* $Rala^{fl/fl}$ and *VillinCreER* $Ralb^{fl/fl}$) to 10 Gy irradiation impaired regenerative capacity when compared to controls (Figure 3F), shown by reduced number and size of regenerating crypts (Figure 3H). Proliferation was also decreased in *Rala*- and *Ralb*-deficient regenerating crypts (Figures 3F and 3H). These data confirmed the conserved role for RALs in regeneration following damage in the adult *Drosophila* and murine intestine.

Next, we investigated whether RAL depletion in the $Lgr5^{+}$ ISC population could block regeneration (Figures 2G–2J). $Rala^{fl/fl}$ and *Lgr5-EGFP-Cre*^{ER} (*Lgr5Cre*^{ER}; Barker et al., 2007) mice were interbred to specifically delete *Rala* in the $Lgr5^{+}$ population. Since the Lgr5CreER transgene exhibits mosaic expression and drives recombination with incomplete penetrance (Leushacke et al., 2017), we employed a robust, 4 day induction regime prior to irradiation (Figure 3E). Use of a *R26-LSL-tdTomato* ($tdTom^{fl}$) reporter strain indicated that recombination occurred in approximately 60% of crypts under this regime (Figure S3I). When *Lgr5-EGFP-Cre*^{ER}; $Rala^{+/+}$ and *Lgr5-EGFP-Cre*^{ER}; $Rala^{fl/fl}$ mice were harvested 72 h post-irradiation, it was observed that *Lgr5-EGFP-Cre*^{ER} $Rala^{fl/fl}$ exhibited significantly fewer regenerating crypts than control animals (Figures 3I and 3J). Importantly, of regenerating crypts within *Lgr5-EGFP-Cre*^{ER} $Rala^{fl/fl}$ intestines, those that had escaped recombination and were *Rala* proficient (Figure 3I) and significantly larger than *Rala*-deficient crypts (Figure 3K).

These experiments confirm a conserved role for RALs in intestinal regeneration, a role directly related to RAL function in *Lgr5*-expressing ISCs.

RAL GTPases Affect Wnt Signaling Activity Upstream of the β-Catenin Destruction Complex in Mice

Given strong evidence of an *in vivo* role for the RALs in regulation of Wnt signaling in *Drosophila* and mice, we investigated which aspect of Wnt signaling was RAL dependent. Initially, since *Rala* or *Ralb* depletion affected the ISC pool in the murine intestine, we predicted that reduction of Wnt ligand would cooperate with RAL deletion to markedly reduce Wnt signaling. To this end, we impaired Wnt ligand secretion using an inhibitor of the O-palmitoyltransferase Porcupine (WNT974) (Figure 4A; Jiang et al., 2013). We have recently shown that this compound has the effect of reducing ISC number *in vivo* (Huels et al., 2018). We observed no significant impact upon normal intestinal viability following continuous treatment for 8 days in *VillinCreER* $Rala^{+/+}$ $Ralb^{+/+}$ mice, but a striking cooperation of RAL deficiency with Porcupine inhibition, whereby *Rala* or *Ralb*-deficient intestines lost intestinal crypts and exhibited reduced proliferation after

(C) Representative image of IHC staining on Cd44, Cleaved Notch1, and β-catenin. Scale bar, 50 μm.
(D) Quantification of IHC staining in 25 crypts per mouse, WT = 5, $Rala^{fl/fl}$ = 4, $Ralb^{fl/fl}$ = 4. Error bars, ± SD.
(E) Experimental design of regeneration experiments in mice following irradiation damage
(F) H&E and BrdU staining on regenerating crypts 3 days after irradiation. White arrows indicate regenerating crypts. Scale bar, 50 μm.
(G) Quantification of crypt numbers and crypt length after irradiation, WT = 5, $Rala^{fl/fl}$ = 4, $Ralb^{fl/fl}$ n = 4. Error bars, ± SD.
(H) Quantification of BrdU positive cells after irradiation, WT = 5, $Rala^{fl/fl}$ = 4, $Ralb^{fl/fl}$ = 4. Error bars, ± SD.
(I) H&E and BrdU staining of regenerating crypts 3 days after irradiation. White arrows indicate regenerating crypts. Scale bar, 50 μm.
(J) Quantification of crypt numbers, and crypt length after irradiation, WT = 4, $Rala^{fl/fl}$ = 5. Error bars, ± SD.
(K) Quantification of crypt size after irradiation in 25 Rala negative and Rala positive crypts based on Rala IHC staining, $Rala^{fl/fl}$ = 5. Mann-Whitney U test. Error bars, ± SD.
Where indicated, Mann-Whitney U test; *$p < 0.05$, **$p < 0.01$.

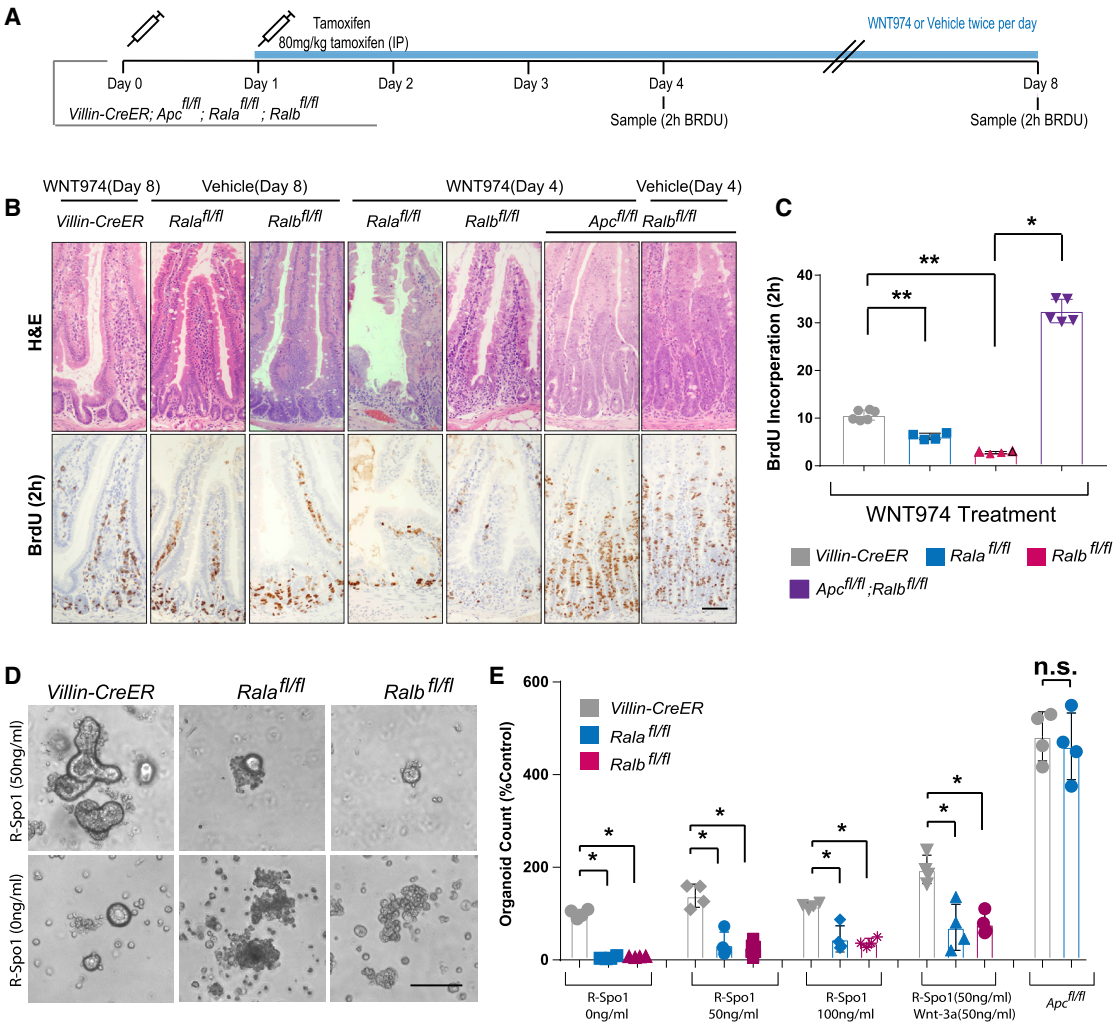

Figure 4. RAL Small GTPase Signaling Acts Upstream of APC in the Wnt Pathway

(A) Design of experiments using Porcupine inhibitor WNT974 in *Rala*$^{fl/fl}$ and *Ralb*$^{fl/fl}$ mice

(B) Representative H&E and BrdU images of small intestine of mice with impaired Ral small GTPase signaling and treated with WNT974. Scale bar, 50 μm.

(C) Quantification of BrdU (50 Crypts per mouse) incorporation in small intestine of *Rala* and *Ralb* conditional knock out mice upon WNT974 treatment, WT = 6, *Rala*$^{fl/fl}$ = 4, *Ralb*$^{fl/fl}$ = 4, and *Apc*$^{fl/fl}$; *Ralb*$^{fl/fl}$ = 5. Error bars, ± SD.

(D) Representative bright field images of organoid growth following *Rala* and *Ralb* deletion and R-spondin1 withdrawal. Scale bar, 50 μm.

(E) Count of viable organoids in culture 72 h after isolation, in media supplemented with 0 ng/mL R-Spo1 (WT = 4, *Rala*$^{fl/fl}$ = 4, and *Ralb*$^{fl/fl}$ = 4), 50 ng/mL R-spo1 (WT = 4, *Rala*$^{fl/fl}$ = 4, and *Ralb*$^{fl/fl}$ = 4), 100 ng/mL R-Spo1 (WT = 4, *Rala*$^{fl/fl}$ = 4, and *Ralb*$^{fl/fl}$ = 4), or 50 ng/mL R-spo1 and 50 ng/mL Wnt-3a (WT = 4, *Rala*$^{fl/fl}$ = 4, and *Ralb*$^{fl/fl}$ = 4), or *APC*$^{fl/fl}$ (WT = 4 and *Ralb*$^{fl/fl}$ = 4). Error bars, ± SD.

Where indicated, Mann-Whitney U test; *p < 0.05, **p < 0.01.

4 days of treatment with WNT974 when compared to controls (Figures 4B and 4C)

Next, we examined whether loss of the destruction complex could rescue the impact of RAL deletion in the context of genetic ablation of the tumor suppressor gene *Apc*, through generation of *VillinCreER; Apc*$^{fl/fl}$*; Ralb*$^{fl/fl}$ mice. Deletion of *Apc* in the entire intestinal epithelium results in a "crypt-progenitor phenotype" characterized by increased proliferation (Sansom et al., 2004), and expression of ISC markers such as *Lgr5* and Wnt target genes, alongside perturbed migration and differentiation. Critically, deletion of *Apc* rescued loss of normal homeostasis and protected *Ralb*-deficient intestines from Porcupine inhibition (Figures 4B and 4C). This indicates that RAL proteins are important for Wnt signaling at the level of the ligand or receptor rather than the destruction complex or transcriptional activation of Wnt target genes in both *Drosophila* and murine intestines.

To expand upon the link between RALs and Wnt signaling, we utilized intestinal organoid culture. Organoids are readily prepared from the intestinal epithelium of mice and grow in a Wnt-dependent manner (Sato et al., 2009). We first cultured organoids from *VillinCreER*; *Rala*$^{fl/fl}$ or *VillinCreER*; *Ralb*$^{fl/fl}$ mice, sampled at 4 days PI. We found that, after 3 days in culture, organoids isolated from *Rala*$^{fl/fl}$ or *Ralb*$^{fl/fl}$ mice exhibited impaired seeding and growth in culture medium supplemented with standard 50 ng/mL R-Spo1 (Figures 4D and 4E). Furthermore, these organoids were inefficient in colony outgrowth (Figure S4A),

implying a loss of stem cell function. To distinguish between establishment and sustained growth of organoids, we next deleted *Ralb* through addition of 1 μM 4-OHT to the culture medium of organoid cultures derived from uninduced *VillinCreER*$^{+}$; *Ralb*$^{fl/fl}$ mice. These organoids rapidly lost the expression of the stem cell marker Cd44 and lost viability at 48 h PI (Figure S4B). Thus, RALs are required for establishment and maintenance of intestinal organoids *in vitro*. Given the that *Rala*- and *Ralb*-deficient crypts were rapidly lost in culture, we questioned whether this was due to ISC differentiation or apoptosis. IHC against cleaved caspase-3 indicated that equivalent levels of apoptosis were present in intestinal crypts of *Rala*- or *Ralb*-deficient mice compared to wild-type (WT) controls *in vivo* (Figures S4C and S4D). This suggests that the loss of ISCs and lack of crypt viability in culture arises from differentiation caused by *Rala* or *Ralb* loss. Given data from *Drosophila*, we predicted that phenotypes driven by *Ralb* depletion in murine intestinal organoids were unlikely to result from impaired production or secretion of Wnt ligands. To test this, we sought to rescue growth of *Ralb*-deficient organoids with exogenous Wnt ligand. Growth was not rescued, suggesting the impact of *Ralb* depletion is not mediated by ligand availability (Figure 4E). In support of *in vivo* observations, *Apc* deficiency restored growth of *Ralb*-deficient organoids (Figure 4E). We also sought to rescue growth by increasing the R-spo1 concentration, which again had no effect on growth (Figure 4E). Interestingly, removing R-spo1 from culture medium impaired growth but did not reduce number of WT organoids, while *Rala*$^{fl/fl}$- and *Ralb*$^{fl/fl}$-derived organoids almost completely failed to seed and grow (Figures 4D and 4E).

RAL GTPase Signaling Mediates Internalization of Frizzled Receptors and Wnt Pathway Activation in HEK293T Cells

RAL depletion had no impact upon Wnt ligand secretion/production in *Drosophila*, and Wnt phenotypes in the fly and mouse were rescued by *Apc* loss, indicating that RALs may regulate receptor complex activation. Given the link between RALs and endocytosis (Jiang et al., 2016; Jullien-Flores et al., 2000), we hypothesized that their role in Wnt signaling may involve regulation of receptor localization. To address this, we deleted *RALA*, *RALB*, and their effector *RALBP1* using CRISPR/Cas9 in HEK293T cells, a well-established model that allows biochemical assessment of Wnt signaling *in vitro* (Figure S5A).

Through analysis of the internalization of biotinylated Frizzled-7 and LRP6 over time, we found that internalization of these Wnt-signalosome receptors was significantly decreased following *RALA*, *RALB*, or *RALBP1* deletion (Figure 5A). This was corroborated through high-resolution imaging of internalization of fluorescently labeled Frizzled-5 or -7 over time (Figure S5B). While the kinetics of Frizzled-5 and and -7 internalization differ, with Frizzled-7 internalized more rapidly under control conditions, internalization of both was reduced following depletion of *RALA*, *RALB*, or *RALBP1* (Figures 5B and 5C). Furthermore, internalization of SNAP-Frizzled-7 was reduced in serum-free medium supplemented with 100 ng/mL Wnt-3a in these lines (Figure 5D), and internalization of biotinylated Frizzled-7 was impaired following *RALA* knockout under the same conditions (Figure 5E). This suggests that RAL GTPases and RALBP1 are involved in regulating Frizzled-7 receptor internalization.

We next assessed canonical Wnt signaling in this setting through accumulation of nuclear β-catenin in nuclear protein fractions as a surrogate. *RALA*, *RALB*, and *RALBP1* depletion resulted in a reduction of nuclear β-catenin when compared to control (Figure 5F). Furthermore, Wnt-3a treatment resulted in a reduction of β-catenin in the cytoplasm of cells with RAL expression (Figure 5F). Moreover, baseline Wnt activity and response to Wnt-3a ligand in *RALA*, *RALB*, and *RALBP1*-depleted lines were reduced as measured by TCF/LEF transcriptional activity using a Super TopFlash construct (Figure 5G).

Given that APC loss rescued lethality caused by RAL depletion in intestinal organoid cultures, APC-deficient organoids can be used to assess the impact of RAL deficiency upon Frizzled receptor internalization. We examined endogenous Frizzled-7 localization through immunofluorescent staining and fluorescence-activated cell sorting (FACS) analysis of cell-surface Frizzled-7 on living disaggregated organoids. Critically, we observed elevation of cell-surface Frizzled-7 expression upon knockout of *Apc and Ralb* in organoids when compared to *Apc* deficiency alone (Figures 5H and 5I). This is supported by higher levels of Frizzled-5, -6, and -7 detected on the cell surface on Ral GTPase knockout HEK293T cells in pull-down experiments (Figure S5D). These data support a role for RAL signaling in activation of Wnt signaling through promotion of internalization of Frizzled-7, and the Wnt signalosome.

RAL GTPases Regulate Stem Cell Function in the Intestine

Next, we explored whether reduced ISC marker expression associated with RAL deletion impacted stem cell fitness when compared to wild-type neighbors. In homeostasis, ISC replacement in the mammalian intestine is a stochastic process, where the presence of competing stem cells eventually results in repopulation of the entire crypt from an individual stem cell (Lopez-Garcia et al., 2010; Snippert et al., 2010). This process is known as neutral drift and is a mechanism for removal of stem cells carrying oncogenic or deleterious mutations (Vermeulen et al., 2013). Indeed, we have shown that reducing the ISC pool increases the likelihood that an oncogenic mutation might overtake the crypt (Huels et al., 2018). These observations suggest that, if Wnt activation in a RAL-deficient stem cell was reduced compared to wild-type neighbors, it would be more likely to be lost within an intestinal crypt over time.

We interbred *Lgr5-EGFP-Cre*^{ER} (*Lgr5Cre*^{ER}) mice (Barker et al., 2007) to *Ralb* conditional knockout, and *R26-LSL-tdTomato* (*tdTom*^{fl}) mice (Madisen et al., 2010), allowing us to visualize expansion of *Ralb*$^{+/fl}$ and *Ralb*$^{fl/fl}$ ISC clones (Figures 6A and 6B). We then induced *Ralb* deletion within individual stem cells per crypt using a low dose of tamoxifen (0.15 mg, in line with established protocols) (Figure 6A). It is notable that, in this system, the induction of *Ralb* deletion in the Lgr5^{+} compartment takes place prior to any impact that *Ralb* has on Wnt-target expression, in particular, *Lgr5*, while expression of TdTomato from the *Rosa26* locus as the readout for the experiment is agnostic of any stem cell marker. Consistently, we observe similar labeling with *tdTom*^{fl} in the presence or absence of *Ralb* at a time point 4 days PI, indicating equal recombination in

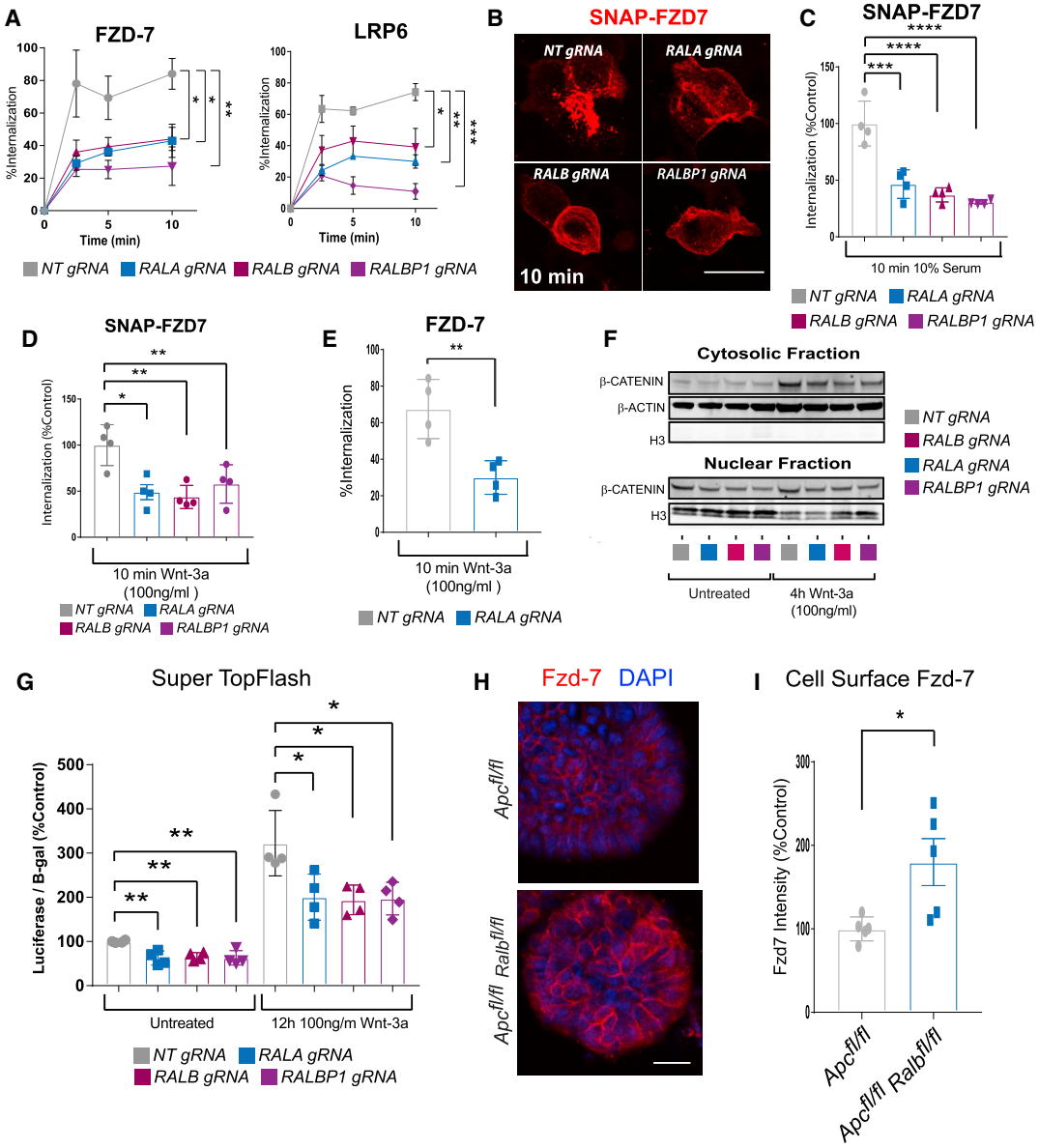

Figure 5. RAL Small GTPase Signaling Mediates Internalization of Frizzled Receptors and Wnt Pathway Activation in HEK293T Cells

(A) HEK293T cells were labeled with NHS-S-S-Biotin at 4°C and internalization allowed to proceed at 37°C. Error bars, ± SEM (3 independent experiments); 1-way ANOVA Tukey's multiple comparisons test.

(B) Representative maximal projection of confocal images of immunofluorescently labeled SNAP-FZD7 after internalization in HEK293T cells. Scale bar, 5 μm.

(C) Quantification of SNAP-FZD7 internalization experiments. Error bars, ± SEM (4 independent experiments); 1-way ANOVA Dunnett's multiple comparisons test.

(D) Quantification of SNAP-FZD7 internalization in serum-free media supplemented with 100 ng/mL Wnt-3a. Error bars, ± SEM (4 independent experiments). 1-way ANOVA Dunnett's multiple comparisons test.

(E) Internalization of NHS-S-S-Biotin-labeled HEK293T in serum-free conditions with Wnt-3a supplemented media. Error bars, ± SEM (4 independent experiments); unpaired t test.

(F) Representative western blots of cytosolic and nuclear β-catenin in HEK293T cell lines following Wnt-3a treatment. β-actin and H3 were used as loading controls. H3 was marked nuclear enrichment.

(G) Wnt activity measured as Super TopFlash luciferase signal normalized to β-galactosidase levels in HEK293t cells following *RALA*, *RALB*, and *RALBP1* knockout and Wnt-3a treatment. Error bars, ± SEM (4 independent experiments). 1-way ANOVA Dunnett's multiple comparisons test.

(H) Immunofluorescence (IF) staining of Fzd-7 in organoids derived from $Apc^{fl/fl}$ = 5, and $Apc^{fl/fl}$, $Ralb^{fl/fl}$ = 5 mice. Scale bar, 50 μm.

(I) Quantification of cell-surface Fzd-7 in organoids using FACS ($Apc^{fl/fl}$ = 5 and $Apc^{fl/fl}$, $Ralb^{fl/fl}$ = 5). Non-parametric Mann-Whitney U test. Error bars, ± SD. Where indicated, *p < 0.05, **p < 0.01, ***p < 0.001, ****p < 0.0001.

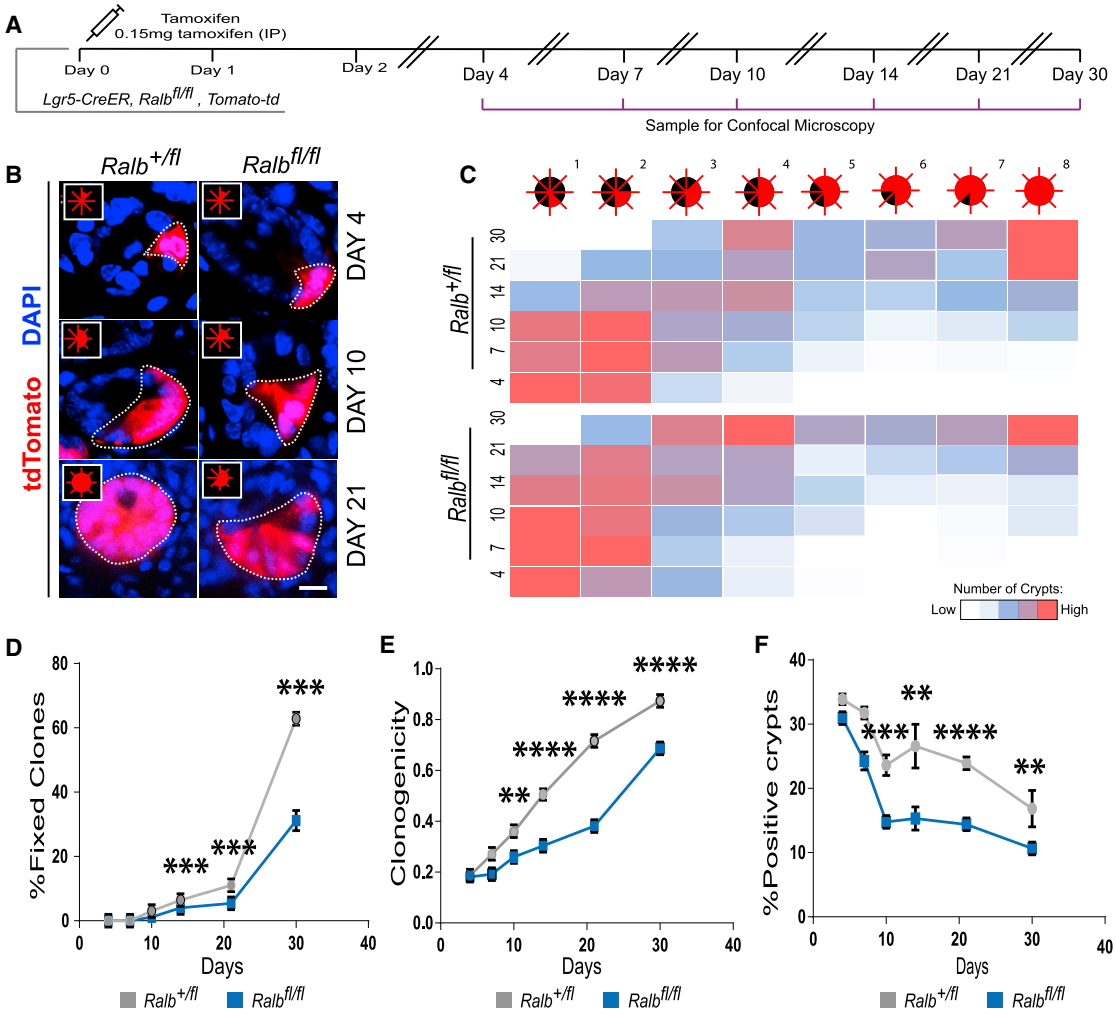

Figure 6. RAL Small GTPases Are Functionally Important for ISCs

(A) Graphical representation of experimental design of clonogenicity experiment

(B) Representative images captured with confocal microscopy of the bottom of intestinal crypts. Scale bar, 5 μm.

(C) Heatmap representing clone size over time after induction in *Ralb*$^{+/fl}$ and *Ralb*$^{fl/fl}$ mice was counted in "eighths." At least 200 clones per mouse were counted (day 4: *Ralb*$^{+/fl}$ = 4, *Ralb*$^{fl/fl}$ = 3; day 7: *Ralb*$^{+/fl}$ = 4, *Ralb*$^{fl/fl}$ = 4; day 10: *Ralb*$^{+/fl}$ = 3, *Ralb*$^{fl/fl}$ = 3; day 14: *Ralb*$^{+/fl}$ = 4, *Ralb*$^{fl/fl}$ = 4; day 21: *Ralb*$^{+/fl}$ = 3, *Ralb*$^{fl/fl}$ = 6; day 21: *Ralb*$^{+/fl}$ = 4, *Ralb*$^{fl/fl}$ = 4).

(D) Average clone size over time in *Ralb* heterozygote and homozygote knockout mice (numbers as in B). Error bars, ± SEM (mean clone size per mouse).

(E) Fully fixed clones over time in *Ralb* heterozygote and homozygote knockout mice (numbers as in B). Error bars, ± SEM (mean fixed clones per mouse).

(F) Quantification of number of tdTomato positive crypts per field. Error bars, ± SEM (mean tdTomato positive crypts per mouse [numbers as in B]).

Where indicated, unpaired t test, **p < 0.01, ***p < 0.001, ****p < 0.0001.

both cases (Figures 6C–6E). However, at later time points (days 10–30) there was a shift to labeled crypts being more sparsely populated in *Ralb*$^{fl/fl}$ mice when compared to *Ralb*$^{+/fl}$ mice, where a substantial proportion of crypts were fully fixed (Figure 6D). Importantly, at day 30 we could confirm that *Ralb* was specifically deleted in fixed tdTomato positive crypts (Figure S6A). Quantification indicated that loss of *Ralb* reduced clonogenicity (Figure 6E) and profoundly reduced the numbers of fully fixed crypts at days 14 and 30 (Figure 6D). Importantly, this resulted in significantly fewer labeled clones in the SI of *Ralb*$^{fl/fl}$ mice (Figure 6F), indicating that depletion of *Ralb* puts ISCs at a disadvantage when compared to wild-type neighbors.

Complete Ablation of RAL GTPase Causes Crypt Death, which Can Be Rescued by APC Loss

Given that our mammalian studies thus far were limited to reduction of global RAL activity through single-gene deletion, we addressed the consequences of ablation of both homologs. We interbred *VillinCreER*; *Rala*$^{fl/fl}$ and VillinCreER; *Ralb*$^{fl/fl}$ strains to generate double *VillinCreER*; *Rala*$^{fl/fl}$; *Ralb*$^{fl/fl}$ conditional mice and induced highly penetrant recombination as before. Deletion of both genes was confirmed by qPCR (Figure S7A). The deletion of both *Rala* and *Ralb* resulted in a dramatic phenotype. At 2 days PI, there was a significant reduction in proliferation (as assessed by bromodeoxyuridine [BrdU] incorporation) (Figures 7A and 7B) and expression of stem cell markers and Wnt target

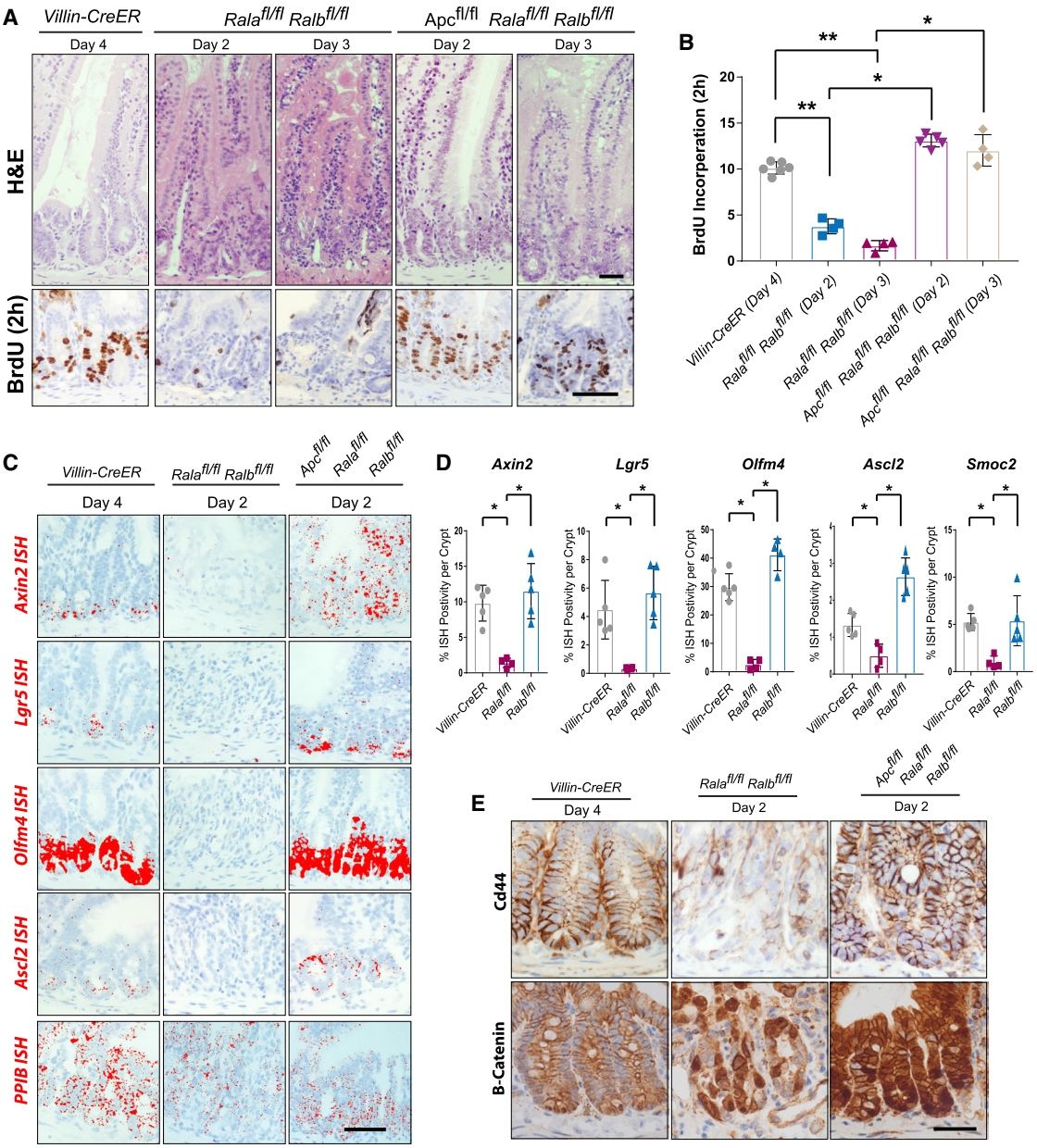

Figure 7. Complete Ablation of RAL GTPase Causes Crypt Death and Can Be Rescued by APC Loss

(A) H&E and BrdU images of small intestine of mice with impaired RAL small GTPase signaling. Scale bar, 50 μm.

(B) Quantification of BrdU (50 crypts per mouse) incorporation in small intestine of *Rala* and *Ralb* conditional knockout mice, in combination or not with *Apc* deletion (WT = 6, day 2: $Rala^{fl/fl}$; $Ralb^{fl/fl}$ = 4, day 3: $Rala^{fl/fl}$; $Ralb^{fl/fl}$ = 4, day 2; $Apc^{fl/fl}$; $Rala^{fl/fl}$; $Ralb^{fl/fl}$ = 5, and day 3: $Apc^{fl/fl}$; $Rala^{fl/fl}$; $Ralb^{fl/fl}$ = 4). Error bars, ± SD. *p < 0.05, **p < 0.01

(C) ISH images on wnt target genes *Axin2*, *Lgr5*, *Olfm4*, and *Ascl2* in the small intestine after *Rala* and *Ralb* deletion in combination or not with *Apc* deletion (Red). *Ppib* used as positive control. Scale bar, 50 μm.

(D) Quantification of ISH staining in 25 crypts per mice (WT = 5, $Rala^{fl/fl}$; $Ralb^{fl/fl}$ = 4, $Apc^{fl/fl}$; $Rala^{fl/fl}$; $Ralb^{fl/fl}$ = 4). Error bars, ± SD. *p < 0.05,

(E) Representative image of IHC staining on Cd44 and β-catenin (WT = 4, $Rala^{fl/fl}$; $Ralb^{fl/fl}$ = 4, $Apc^{fl/fl}$; $Rala^{fl/fl}$; $Ralb^{fl/fl}$ = 4). Scale bar, 50 μm.

Where indicated, Mann-Whitney U test, *p < 0.05, **p < 0.01.

genes (Figures 7C, 7D, and S7B), albeit with no significant increase in cleaved caspase-3 positive cells (Figures S7C and S7D). At 3 days PI, crypt structures were absent, indicating functional loss of stem cells within the intestine (Figure 7A), while goblet and Paneth cell numbers remained unaffected (Figure S7C), although Paneth cell localization shifted toward the intestinal lumen as crypts were lost. Given the promiscuous nature of RAL signaling, we sought to confirm whether crypt loss following complete genetic ablation of *Rala* and *Ralb* was related to suppression of Wnt signaling, again by assessing whether

deletion of Apc could rescue the phenotype. Remarkably, crypt architecture was maintained in intestines from *VillinCreER; Apc$^{fl/fl}$; Rala$^{fl/fl}$; Ralb$^{fl/fl}$* mice, and intestinal crypts exhibited significant proliferation (Figures 7A and 7B), alongside expression of Wnt targets and ISC markers such as *Lgr5*, *Olfm4*, *Axin2*, *Ascl2*, β-catenin, and Cd44 (Figures 7C–7E).

DISCUSSION

We present a conserved *in vivo* role for RAL signaling in regulating ISC number, which impacts intestinal homeostasis and regeneration. RALs do so by promoting internalization of the Wnt pathway receptor complex at the cell surface, and activating canonical Wnt signaling.

RAL GTPases and the Potentiation of Wnt Signaling in the Intestine

Studies have demonstrated that Wnt and Rspo interact to drive ISC expansion and maintenance in the intestine (Yan et al., 2017). Our work suggests that loss of RAL expression reduces Wnt pathway activity and results in differentiation of Lgr5$^+$ stem cells, no longer agonized by Rspo. The result would be an intestine with significantly fewer functional ISCs. It should be noted we see a dramatic impact on Frizzled-7 internalization *in vitro*, and that this receptor is also highly expressed in ISCs. Loss of frizzled 7 also causes specific loss of Lgr5$^+$ ISC (Flanagan et al., 2015).

The non-redundant role of mammalian *Rala* and *Ralb* (Peschard et al., 2012) is consistent with our previous observations of single-gene knockdown having essential functions during regeneration of the intestine, while redundant for normal tissue homeostasis (Ashton et al., 2010; Cordero et al., 2014). This implies that the threshold of Wnt signaling required for homeostatic stem cell renewal may differ from that required for intestinal regeneration. Consistently, during regeneration, where Wnt signaling and stem cell function must be potentiated, the effect of the loss of either RAL isoform is more apparent. Similarly, further reduction in Wnt ligand through Porcupine inhibition strongly enhances the effects of partial *Ral* loss of function in the intestine, resulting in a complete loss of stem cell function and ultimately crypt death. Critically, total ablation of *Rala* and *Ralb* is likely to reduce Wnt signaling below a threshold level required for intestinal survival, mimicking the effect of β-catenin deletion or DKK overexpression (Ireland et al., 2004; Kuhnert et al., 2004).

RAL Proteins Function Upstream of β-Catenin Activation in the Intestine

Our data provide robust *in vivo* evidence of the impact of altered Wnt signaling beyond direct control of β-catenin stability by the destruction complex (Figure 3). More precisely, it emphasizes the value of restricting the cellular localization of pathway receptors (Figure 4). The robust rescue of both fly and murine RAL loss of function phenotypes through depletion of *Apc* suggests that within ISCs, control of Wnt signaling by RAL is a dominant event. This mirrors the phenotype observed following combined deletion of GSK3α and GSK3β in the intestine, which mimics that of *Apc* loss despite the non-Wnt-related functions of these kinases (Huels et al., 2015).

RAL GTPases and the Regulation of Signaling Pathways through Receptor Internalization

Our study strongly suggests that endocytosis driven by RAL and RALBP1 is critical for Wnt activity *in vivo*. A previous study suggested that the active Wnt signalosome resides within Clathrin-mediated pits (Gammons et al., 2016), while others indicate that caveolar endocytosis is important for Wnt pathway activation (Blitzer and Nusse, 2006; Yamamoto et al., 2006). These differences in part seem to be determined by cell type (Feng and Gao, 2015; Kim et al., 2013). Previously, RALBP1 has been associated with Clathrin-mediated endocytosis (Jullien-Flores et al., 2000), while the RALs have also been linked to caveolar endocytosis (Jiang et al., 2016). These studies indicate that RALs have general role controlling endocytic processes. Recently, the Wnt-regulatory tumor suppressor APC has also been postulated to inhibit Clathrin-mediated endocytosis, whereupon impairment of APC allows cells to use Clathrin-mediated endocytosis to drive ligand independent activation of the receptors (Saito-Diaz et al., 2018). In addition to a better understanding of the specific role of RAL signaling in endocytosis, there is a need to elucidate the contribution of clathrin and non-clathrin-mediated endocytosis on Wnt signaling in both ISCs and CRC.

A Conserved Role of RAL GTPases in the Intestine

Most RAL-dependent intestinal phenotypes analyzed in our studies are conserved between *Drosophila* and mice. One difference is the role of RAL in homeostasis, which appears redundant in the fly, at least in the context of partial knockdown by RNAi. This may relate to differences in homeostatic proliferative state between the two model systems. In the fly midgut, basal stem cell proliferation is low and there is no transit amplifying proliferative zone (Micchelli and Perrimon, 2006; Ohlstein and Spradling, 2006), while Wnt signaling pathway activity within ISCs/EBs in the fly midgut is barely detectable in homeostatic conditions. In contrast, there is very high basal Wnt signaling in mammalian Lgr5$^+$ ISCs, which are as a result, rapidly impacted following *Rala* or *Ralb* depletion. Our previous studies have shown that Wg is significantly induced during regeneration in the adult *Drosophila* midgut, where we also see the dramatic impact of *Ral* knockdown (Cordero et al., 2012b; Figure 1). Despite differences in the two model systems, our results clearly demonstrate the power of combining *Drosophila* and mouse models to understand fundamental principles of ISC biology.

We detail a conserved functional role for the RALs for ISC regeneration. Importantly, our work points to the regulation of cell-surface receptor complex internalization as a mechanism to maintain Wnt signaling and stem cell responses to the proliferative demands of the intestine.

STAR★METHODS

Detailed methods are provided in the online version of this paper and include the following:

- KEY RESOURCES TABLE
- CONTACT FOR REAGENT AND RESOURCE SHARING
- EXPERIMENTAL MODEL AND SUBJECT DETAILS
  - Experimental Animals
  - *Drosophila* breeding and maintenance

SUPPLEMENTAL INFORMATION

Supplemental Information can be found with this article online at https://doi.org/10.1016/j.stem.2019.02.002.

ACKNOWLEDGMENTS

We thank Colin Nixon, the histology service, biological services, and all core services at CRUK Beatson Institute for their invaluable assistance. We thank Prof. Mariann Bienz and Dr. Melissa Gammons for SNAP-tag constructs. We thank Prof. Jim Norman for expertise in receptor internalization. We also thank Bruno Lemaitre, Gaiti Hasan, Hugo Bellen, Ginés Morata, Christian Ghiglione, the Vienna *Drosophila* RNAi Center, the Bloomington *Drosophila* Stock Center, and the Developmental Studies Hybridoma Bank for providing *Drosophila* lines and reagents. This work was supported by CRUK core funding to O.J.S. (A19196 and A21139) (J.J., M.C.H., K.A.P., B.W.M., R.A.R., A.D.C., and O.J.S.). J.J. and K.A.P. were funded as part of a collaborative research agreement with Novartis AG. M.N. is supported by a Leadership Fellowship from the University of Glasgow (to J.B.C.). Y.Y. is supported by CRUK core funding (A17196). J.B.C. is a Sir Henry Dale Fellow jointly funded by the Wellcome Trust and the Royal Society (grant number 104103/Z/14/Z).

AUTHOR CONTRIBUTIONS

J.J., M.N., K.A.P., B.W.M., Y.Y., and R.R. performed experiments. J.J., M.N., M.C.H., R.R., B.W.M., P.P., S.B., A.D.C., J.B.C., and O.J.S. designed experiments and analyzed the data. J.J., M.N., A.D.C., J.B.C., and O.J.S. wrote the manuscript. J.B.C. and O.J.S. directed the study.

DECLARATION OF INTERESTS

The authors declare no competing interests.

Received: July 11, 2018
Revised: December 24, 2018
Accepted: February 5, 2019
Published: March 7, 2019

REFERENCES

Ahmed, Y., Hayashi, S., Levine, A., and Wieschaus, E. (1998). Regulation of armadillo by a Drosophila APC inhibits neuronal apoptosis during retinal development. Cell *93*, 1171–1182.

Ashton, G.H., Morton, J.P., Myant, K., Phesse, T.J., Ridgway, R.A., Marsh, V., Wilkins, J.A., Athineos, D., Muncan, V., Kemp, R., et al. (2010). Focal adhesion kinase is required for intestinal regeneration and tumorigenesis downstream of Wnt/c-Myc signaling. Dev. Cell *19*, 259–269.

Barker, N., van Es, J.H., Kuipers, J., Kujala, P., van den Born, M., Cozijnsen, M., Haegebarth, A., Korving, J., Begthel, H., Peters, P.J., and Clevers, H. (2007). Identification of stem cells in small intestine and colon by marker gene Lgr5. Nature *449*, 1003–1007.

Basset, A., Khush, R.S., Braun, A., Gardan, L., Boccard, F., Hoffmann, J.A., and Lemaitre, B. (2000). The phytopathogenic bacteria Erwinia carotovora infects Drosophila and activates an immune response. Proc. Natl. Acad. Sci. USA *97*, 3376–3381.

Bilic, J., Huang, Y.L., Davidson, G., Zimmermann, T., Cruciat, C.M., Bienz, M., and Niehrs, C. (2007). Wnt induces LRP6 signalosomes and promotes dishevelled-dependent LRP6 phosphorylation. Science *316*, 1619–1622.

Blitzer, J.T., and Nusse, R. (2006). A critical role for endocytosis in Wnt signaling. BMC Cell Biol. *7*, 28.

Bodemann, B.O., and White, M.A. (2008). Ral GTPases and cancer: linchpin support of the tumorigenic platform. Nat. Rev. Cancer *8*, 133–140.

Bourbon, H.M., Gonzy-Treboul, G., Peronnet, F., Alin, M.F., Ardourel, C., Benassayag, C., Cribbs, D., Deutsch, J., Ferrer, P., Haenlin, M., et al. (2002). A P-insertion screen identifying novel X-linked essential genes in Drosophila. Mech. Dev. *110*, 71–83.

Casali, A., and Batlle, E. (2009). Intestinal stem cells in mammals and Drosophila. Cell Stem Cell *4*, 124–127.

Chen, X.W., Leto, D., Chiang, S.H., Wang, Q., and Saltiel, A.R. (2007). Activation of RalA is required for insulin-stimulated Glut4 trafficking to the plasma membrane via the exocyst and the motor protein Myo1c. Dev. Cell *13*, 391–404.

Chien, Y., Kim, S., Bumeister, R., Loo, Y.M., Kwon, S.W., Johnson, C.L., Balakireva, M.G., Romeo, Y., Kopelovich, L., Gale, M., Jr., et al. (2006). RalB GTPase-mediated activation of the IkappaB family kinase TBK1 couples innate immune signaling to tumor cell survival. Cell *127*, 157–170.

Chung, S.S., Lee, J.S., Kim, M., Ahn, B.Y., Jung, H.S., Lee, H.M., Kim, J.W., and Park, K.S. (2012). Regulation of Wnt/β-catenin signaling by CCAAT/enhancer binding protein β during adipogenesis. Obesity (Silver Spring) *20*, 482–487.

Clevers, H. (2006). Wnt/beta-catenin signaling in development and disease. Cell *127*, 469–480.

Cordero, J.B., Stefanatos, R.K., Myant, K., Vidal, M., and Sansom, O.J. (2012a). Non-autonomous crosstalk between the Jak/Stat and Egfr pathways mediates Apc1-driven intestinal stem cell hyperplasia in the Drosophila adult midgut. Development *139*, 4524–4535.

Cordero, J.B., Stefanatos, R.K., Scopelliti, A., Vidal, M., and Sansom, O.J. (2012b). Inducible progenitor-derived Wingless regulates adult midgut regeneration in Drosophila. EMBO J. *31*, 3901–3917.

Cordero, J.B., Ridgway, R.A., Valeri, N., Nixon, C., Frame, M.C., Muller, W.J., Vidal, M., and Sansom, O.J. (2014). c-Src drives intestinal regeneration and transformation. EMBO J. *33*, 1474–1491.

Degirmenci, B., Valenta, T., Dimitrieva, S., Hausmann, G., and Basler, K. (2018). GLI1-expressing mesenchymal cells form the essential Wnt-secreting niche for colon stem cells. Nature *558*, 449–453.

Dutta, D., Buchon, N., Xiang, J., and Edgar, B.A. (2015). Regional Cell Specific RNA Expression Profiling of FACS Isolated Drosophila Intestinal Cell Populations. Curr. Protoc. Stem Cell Biol. *34*, 1–14.

el Marjou, F., Janssen, K.P., Chang, B.H., Li, M., Hindie, V., Chan, L., Louvard, D., Chambon, P., Metzger, D., and Robine, S. (2004). Tissue-specific and inducible Cre-mediated recombination in the gut epithelium. Genesis *39*, 186–193.

Feng, Q., and Gao, N. (2015). Keeping Wnt signalosome in check by vesicular traffic. J. Cell. Physiol. *230*, 1170–1180.

Flanagan, D.J., Phesse, T.J., Barker, N., Schwab, R.H., Amin, N., Malaterre, J., Stange, D.E., Nowell, C.J., Currie, S.A., Saw, J.T., et al. (2015). Frizzled7

functions as a Wnt receptor in intestinal epithelial Lgr5(+) stem cells. Stem Cell Reports *4*, 759–767.

Furriols, M., and Bray, S. (2001). A model Notch response element detects Suppressor of Hairless-dependent molecular switch. Curr. Biol. *11*, 60–64.

Gammons, M.V., Renko, M., Johnson, C.M., Rutherford, T.J., and Bienz, M. (2016). Wnt Signalosome Assembly by DEP Domain Swapping of Dishevelled. Mol. Cell *64*, 92–104.

González-García, A., Pritchard, C.A., Paterson, H.F., Mavria, G., Stamp, G., and Marshall, C.J. (2005). RalGDS is required for tumor formation in a model of skin carcinogenesis. Cancer Cell *7*, 219–226.

Goto, S., and Hayashi, S. (1999). Proximal to distal cell communication in the Drosophila leg provides a basis for an intercalary mechanism of limb patterning. Development *126*, 3407–3413.

Gregorieff, A., Pinto, D., Begthel, H., Destrée, O., Kielman, M., and Clevers, H. (2005). Expression pattern of Wnt signaling components in the adult intestine. Gastroenterology *129*, 626–638.

Herranz, H., Perez, L., Martin, F.A., and Milan, M. (2008). A Wingless and Notch double-repression mechanism regulates G1-S transition in the Drosophila wing. EMBO J. *27*, 1633–1645.

Huels, D.J., Ridgway, R.A., Radulescu, S., Leushacke, M., Campbell, A.D., Biswas, S., Leedham, S., Serra, S., Chetty, R., Moreaux, G., et al. (2015). E-cadherin can limit the transforming properties of activating β-catenin mutations. EMBO J. *34*, 2321–2333.

Huels, D.J., Bruens, L., Hodder, M.C., Cammareri, P., Campbell, A.D., Ridgway, R.A., Gay, D.M., Solar-Abboud, M., Faller, W.J., Nixon, C., et al. (2018). Wnt ligands influence tumour initiation by controlling the number of intestinal stem cells. Nat. Commun. *9*, 1132.

Ireland, H., Kemp, R., Houghton, C., Howard, L., Clarke, A.R., Sansom, O.J., and Winton, D.J. (2004). Inducible Cre-mediated control of gene expression in the murine gastrointestinal tract: effect of loss of beta-catenin. Gastroenterology *126*, 1236–1246.

Jiang, H., Patel, P.H., Kohlmaier, A., Grenley, M.O., McEwen, D.G., and Edgar, B.A. (2009). Cytokine/Jak/Stat signaling mediates regeneration and homeostasis in the Drosophila midgut. Cell *137*, 1343–1355.

Jiang, X., Hao, H.X., Growney, J.D., Woolfenden, S., Bottiglio, C., Ng, N., Lu, B., Hsieh, M.H., Bagdasarian, L., Meyer, R., et al. (2013). Inactivating mutations of RNF43 confer Wnt dependency in pancreatic ductal adenocarcinoma. Proc. Natl. Acad. Sci. USA *110*, 12649–12654.

Jiang, Y., Sverdlov, M.S., Toth, P.T., Huang, L.S., Du, G., Liu, Y., Natarajan, V., and Minshall, R.D. (2016). Phosphatidic Acid Produced by RalA-activated PLD2 Stimulates Caveolae-mediated Endocytosis and Trafficking in Endothelial Cells. J. Biol. Chem. *291*, 20729–20738.

Jullien-Flores, V., Mahé, Y., Mirey, G., Leprince, C., Meunier-Bisceuil, B., Sorkin, A., and Camonis, J.H. (2000). RLIP76, an effector of the GTPase Ral, interacts with the AP2 complex: involvement of the Ral pathway in receptor endocytosis. J. Cell Sci. *113*, 2837–2844.

Kim, T.H., Escudero, S., and Shivdasani, R.A. (2012). Intact function of Lgr5 receptor-expressing intestinal stem cells in the absence of Paneth cells. Proc. Natl. Acad. Sci. USA *109*, 3932–3937.

Kim, I., Pan, W., Jones, S.A., Zhang, Y., Zhuang, X., and Wu, D. (2013). Clathrin and AP2 are required for PtdIns(4,5)P2-mediated formation of LRP6 signalosomes. J. Cell Biol. *200*, 419–428.

Kishida, S., Yamamoto, H., Hino, S., Ikeda, S., Kishida, M., and Kikuchi, A. (1999). DIX domains of Dvl and axin are necessary for protein interactions and their ability to regulate beta-catenin stability. Mol. Cell. Biol. *19*, 4414–4422.

Koo, B.K., Spit, M., Jordens, I., Low, T.Y., Stange, D.E., van de Wetering, M., van Es, J.H., Mohammed, S., Heck, A.J.R., Maurice, M.M., et al. (2012). Tumour suppressor RNF43 is a stem-cell E3 ligase that induces endocytosis of Wnt receptors. Nature *488*, 665–669.

Koyama, S., and Kikuchi, A. (2001). Ras interaction with RalGDS effector targets. Methods Enzymol. *332*, 127–138.

Kuhnert, F., Davis, C.R., Wang, H.T., Chu, P., Lee, M., Yuan, J., Nusse, R., and Kuo, C.J. (2004). Essential requirement for Wnt signaling in proliferation of adult small intestine and colon revealed by adenoviral expression of Dickkopf-1. Proc. Natl. Acad. Sci. USA *101*, 266–271.

Lee, T., and Luo, L. (1999). Mosaic analysis with a repressible cell marker for studies of gene function in neuronal morphogenesis. Neuron *22*, 451–461.

Lee, T., and Luo, L. (2001). Mosaic analysis with a repressible cell marker (MARCM) for Drosophila neural development. Trends Neurosci. *24*, 251–254.

Lemaitre, B., and Miguel-Aliaga, I. (2013). The digestive tract of Drosophila melanogaster. Annu. Rev. Genet. *47*, 377–404.

Leushacke, M., Tan, S.H., Wong, A., Swathi, Y., Hajamohideen, A., Tan, L.T., Goh, J., Wong, E., Denil, S.L.I.J., Murakami, K., and Barker, N. (2017). Lgr5-expressing chief cells drive epithelial regeneration and cancer in the oxyntic stomach. Nat. Cell Biol. *19*, 774–786.

Lim, K.H., Baines, A.T., Fiordalisi, J.J., Shipitsin, M., Feig, L.A., Cox, A.D., Der, C.J., and Counter, C.M. (2005). Activation of RalA is critical for Ras-induced tumorigenesis of human cells. Cancer Cell *7*, 533–545.

Lin, G., Xu, N., and Xi, R. (2008). Paracrine Wingless signalling controls self-renewal of Drosophila intestinal stem cells. Nature *455*, 1119–1123.

Lopez-Garcia, C., Klein, A.M., Simons, B.D., and Winton, D.J. (2010). Intestinal stem cell replacement follows a pattern of neutral drift. Science *330*, 822–825.

MacDonald, B.T., Tamai, K., and He, X. (2009). Wnt/beta-catenin signaling: components, mechanisms, and diseases. Dev. Cell *17*, 9–26.

Madisen, L., Zwingman, T.A., Sunkin, S.M., Oh, S.W., Zariwala, H.A., Gu, H., Ng, L.L., Palmiter, R.D., Hawrylycz, M.J., Jones, A.R., et al. (2010). A robust and high-throughput Cre reporting and characterization system for the whole mouse brain. Nat. Neurosci. *13*, 133–140.

Martin, T.D., Samuel, J.C., Routh, E.D., Der, C.J., and Yeh, J.J. (2011). Activation and involvement of Ral GTPases in colorectal cancer. Cancer Res. *71*, 206–215.

Metcalfe, C., Kljavin, N.M., Ybarra, R., and de Sauvage, F.J. (2014). Lgr5+ stem cells are indispensable for radiation-induced intestinal regeneration. Cell Stem Cell *14*, 149–159.

Micchelli, C.A., and Perrimon, N. (2006). Evidence that stem cells reside in the adult Drosophila midgut epithelium. Nature *439*, 475–479.

Nászai, M., Carroll, L.R., and Cordero, J.B. (2015). Intestinal stem cell proliferation and epithelial homeostasis in the adult Drosophila midgut. Insect Biochem. Mol. Biol. *67*, 9–14.

Neel, N.F., Martin, T.D., Stratford, J.K., Zand, T.P., Reiner, D.J., and Der, C.J. (2011). The RalGEF-Ral Effector Signaling Network: The Road Less Traveled for Anti-Ras Drug Discovery. Genes Cancer *2*, 275–287.

Neyen, C., Bretscher, A.J., Binggeli, O., and Lemaitre, B. (2014). Methods to study Drosophila immunity. Methods *68*, 116–128.

Nolo, R., Abbott, L.A., and Bellen, H.J. (2000). Senseless, a Zn finger transcription factor, is necessary and sufficient for sensory organ development in Drosophila. Cell *102*, 349–362.

Ohlstein, B., and Spradling, A. (2006). The adult Drosophila posterior midgut is maintained by pluripotent stem cells. Nature *439*, 470–474.

Olson, E.R., Pancratov, R., Chatterjee, S.S., Changkakoty, B., Pervaiz, Z., and DasGupta, R. (2011). Yan, an ETS-domain transcription factor, negatively modulates the Wingless pathway in the Drosophila eye. EMBO Rep. *12*, 1047–1054.

Peschard, P., McCarthy, A., Leblanc-Dominguez, V., Yeo, M., Guichard, S., Stamp, G., and Marshall, C.J. (2012). Genetic deletion of RALA and RALB small GTPases reveals redundant functions in development and tumorigenesis. Curr. Biol. *22*, 2063–2068.

Richhariya, S., Jayakumar, S., Abruzzi, K., Rosbash, M., and Hasan, G. (2017). A pupal transcriptomic screen identifies Ral as a target of store-operated calcium entry in Drosophila neurons. Sci. Rep. *7*, 42586.

Rodriguez-Viciana, P., and McCormick, F. (2005). RalGDS comes of age. Cancer Cell *7*, 205–206.

Saha, S., Aranda, E., Hayakawa, Y., Bhanja, P., Atay, S., Brodin, N.P., Li, J., Asfaha, S., Liu, L., Tailor, Y., et al. (2016). Macrophage-derived extracellular vesicle-packaged WNTs rescue intestinal stem cells and enhance survival after radiation injury. Nat. Commun. *7*, 13096.

Saito-Diaz, K., Benchabane, H., Tiwari, A., Tian, A., Li, B., Thompson, J.J., Hyde, A.S., Sawyer, L.M., Jodoin, J.N., Santos, E., et al. (2018). APC Inhibits Ligand-Independent Wnt Signaling by the Clathrin Endocytic Pathway. Dev. Cell *44*, 566–581.

Sansom, O.J., Reed, K.R., Hayes, A.J., Ireland, H., Brinkmann, H., Newton, I.P., Batlle, E., Simon-Assmann, P., Clevers, H., Nathke, I.S., et al. (2004). Loss of Apc in vivo immediately perturbs Wnt signaling, differentiation, and migration. Genes Dev. *18*, 1385–1390.

Sato, T., Vries, R.G., Snippert, H.J., van de Wetering, M., Barker, N., Stange, D.E., van Es, J.H., Abo, A., Kujala, P., Peters, P.J., and Clevers, H. (2009). Single Lgr5 stem cells build crypt-villus structures in vitro without a mesenchymal niche. Nature *459*, 262–265.

Sato, T., van Es, J.H., Snippert, H.J., Stange, D.E., Vries, R.G., van den Born, M., Barker, N., Shroyer, N.F., van de Wetering, M., and Clevers, H. (2011). Paneth cells constitute the niche for Lgr5 stem cells in intestinal crypts. Nature *469*, 415–418.

Schwarz-Romond, T., Fiedler, M., Shibata, N., Butler, P.J., Kikuchi, A., Higuchi, Y., and Bienz, M. (2007). The DIX domain of Dishevelled confers Wnt signaling by dynamic polymerization. Nat. Struct. Mol. Biol. *14*, 484–492.

Shoshkes-Carmel, M., Wang, Y.J., Wangensteen, K.J., Tóth, B., Kondo, A., Massasa, E.E., Itzkovitz, S., and Kaestner, K.H. (2018). Subepithelial telocytes are an important source of Wnts that supports intestinal crypts. Nature *557*, 242–246.

Snippert, H.J., van der Flier, L.G., Sato, T., van Es, J.H., van den Born, M., Kroon-Veenboer, C., Barker, N., Klein, A.M., van Rheenen, J., Simons, B.D., and Clevers, H. (2010). Intestinal crypt homeostasis results from neutral competition between symmetrically dividing Lgr5 stem cells. Cell *143*, 134–144.

Snippert, H.J., Schepers, A.G., van Es, J.H., Simons, B.D., and Clevers, H. (2014). Biased competition between Lgr5 intestinal stem cells driven by oncogenic mutation induces clonal expansion. EMBO Rep. *15*, 62–69.

Strigini, M., and Cohen, S.M. (2000). Wingless gradient formation in the Drosophila wing. Curr. Biol. *10*, 293–300.

Valenta, T., Degirmenci, B., Moor, A.E., Herr, P., Zimmerli, D., Moor, M.B., Hausmann, G., Cantù, C., Aguet, M., and Basler, K. (2016). Wnt Ligands Secreted by Subepithelial Mesenchymal Cells Are Essential for the Survival of Intestinal Stem Cells and Gut Homeostasis. Cell Rep. *15*, 911–918.

Vermeulen, L., Morrissey, E., van der Heijden, M., Nicholson, A.M., Sottoriva, A., Buczacki, S., Kemp, R., Tavaré, S., and Winton, D.J. (2013). Defining stem cell dynamics in models of intestinal tumor initiation. Science *342*, 995–998.

Wang, L., Zeng, X., Ryoo, H.D., and Jasper, H. (2014). Integration of UPRER and oxidative stress signaling in the control of intestinal stem cell proliferation. PLoS Genetics *10*, e1004568.

Yamamoto, H., Komekado, H., and Kikuchi, A. (2006). Caveolin is necessary for Wnt-3a-dependent internalization of LRP6 and accumulation of β-catenin. Dev. Cell *11*, 213–223.

Yan, C., Liu, D., Li, L., Wempe, M.F., Guin, S., Khanna, M., Meier, J., Hoffman, B., Owens, C., Wysoczynski, C.L., et al. (2014). Discovery and characterization of small molecules that target the GTPase Ral. Nature *515*, 443–447.

Yan, K.S., Janda, C.Y., Chang, J., Zheng, G.X.Y., Larkin, K.A., Luca, V.C., Chia, L.A., Mah, A.T., Han, A., Terry, J.M., et al. (2017). Non-equivalence of Wnt and R-spondin ligands during Lgr5^{+} intestinal stem-cell self-renewal. Nature *545*, 238–242.

Zeng, X., Chauhan, C., and Hou, S.X. (2010). Characterization of midgut stem cell- and enteroblast-specific Gal4 lines in Drosophila. Genesis *48*, 607–611.

Zou, W.Y., Blutt, S.E., Zeng, X.L., Chen, M.S., Lo, Y.H., Castillo-Azofeifa, D., Klein, O.D., Shroyer, N.F., Donowitz, M., and Estes, M.K. (2018). Epithelial WNT Ligands Are Essential Drivers of Intestinal Stem Cell Activation. Cell Rep. *22*, 1003–1015.

STAR★METHODS

KEY RESOURCES TABLE

REAGENT or RESOURCE	SOURCE	IDENTIFIER
Antibodies		
mouse monoclonal anti *Drosophila* Armadillo	DSHB	Cat# N2 7A1 ARMADILLO; RRID:AB_528089
mouse monoclonal anti *Drosophila* Prospero	DSHB	Cat# Prospero (MR1A); RRID:AB_528440
chicken polyclonal anti GFP	AbCam	Cat# ab13970; RRID:AB_300798
rabbit polyclonal anti Phospho-Histone H3 (Ser10)	Cell Signaling Technology	Cat# 9701; RRID:AB_331535
mouse monoclonal anti *Drosophila* Wg	DSHB	Cat# 4d4; RRID:AB_528512
rabbit polyclonal anti DsRed	Clontech Laboratories, Inc.	Cat# 632496; RRID:AB_10013483
guinea pig polyclonal anti *Drosophila* Senseless	H. Bellen; (Nolo et al., 2000)	N/A
guinea pig polyclonal anti *Drosophila* Myc	G. Morata; (Herranz et al., 2008)	N/A
rabbit polyclonal anti β-Galactosidase	MP Biomedicals	Cat# 559761; RRID:AB_2687418
goat anti-chicken-IgY(H+L)-Alexa Fluor 488	Invitrogen	Cat# A-11039; RRID:AB_142924
goat anti-mouse-IgG(H+L)-Alexa Fluor 488	Molecular Probes	Cat# A-11029; RRID:AB_138404
goat anti-guinea pig-IgG(H+L)-Alexa Fluor 488	Thermo Fisher Scientific	Cat# A-11073; RRID:AB_2534117
goat anti-rabbit-IgG(H+L)-Alexa Fluor 594	Thermo Fisher Scientific	Cat# A-11037; RRID:AB_2534095
goat anti-mouse-IgG(H+L)-Alexa Fluor 594	Molecular Probes	Cat# A-11032; RRID:AB_141672
goat anti-guinea pig-IgG(H+L)-Alexa Fluor 594	Thermo Fisher Scientific	Cat# A-11076; RRID:AB_2534120
goat anti-guinea pig IgG(H+L)-Alexa Fluor 647	Thermo Fisher Scientific	Cat# A-21450; RRID:AB_2735091
Mouse anti-BrdU	BD Biosciences	Cat# 51-75512X, RRID:AB_2314034
Rat anti-CD44	Bd Bioscience	Cat# 550538, RRID:AB_393732
Rabbit anti-Frizzled-5	LSBio	Cat# LS-A4273, RRID:AB_591417
Rabbit anti-Frizzled-6	GeneTex	Cat.No: GTX64757
Rabbit anti-Frizzled-7	Abcam	Cat# ab64636, RRID:AB_1640522
Rabbit anti- Frizzled-7	LSBio	Cat# LS-C30350, RRID:AB_2263257
Mouse anti-RALA	BD Biosciences	Cat# 610222, RRID:AB_397619
Mouse anti-RALB	Millipore	Cat# 04-037, RRID:AB_612061
Rabbit anti-RALBP1	Abcam	Cat# ab33446, RRID:AB_945151
Mouse anti-B-Actin	Sigma-Aldrich	Cat# A2228, RRID:AB_476697
Rabbit anti-Histone H3	Millipore	Cat# 06-599, RRID:AB_2115283
Rabbit anti-RFP	Tebu-bio, UK	Cat# 600-401-379, RRID:AB_2209751
Rabbit anti-Cleaved Caspase-3	Cell Signaling	Cat# 9661, RRID:AB_2341188
Rabbit anti-lrp6	Abcam	Cat# ab134146
Mouse anti-β-catenin	BD Biosciences	Cat# 610153, RRID:AB_397554
Rabbit anti-Notch1	Cell Signaling	Cat# 2421, RRID:AB_2314204
Bacterial and Virus Strains		
Erwinia carotovora carotovora 15	B. Lemaitre; (Basset et al., 2000)	N/A
Chemicals, Peptides, and Recombinant Proteins		
High Capacity cDNA Reverse Transcription Kit	Applied Biosystems	Cat# 4368813
MessageBOOSTER cDNA Synthesis Kit	Lucigen	Cat# MB060124
PerfeCTa SYBR Green FastMix (Low ROX)	Quanta Bio	Cat# 95074-012
VECTASHIELD Mounting Medium with DAPI	Vector Laboratories, Inc.	Cat# H-1200; RRID:AB_2336790
Critical Commercial Assays		
RNAeasy Mini Kit (50)	QIAGEN	Cat# 74104
Experimental Models: Cell Lines		
HEK293T cells	ATCC	RRID: CVCL_0063

(*Continued on next page*)

Continued

REAGENT or RESOURCE	SOURCE	IDENTIFIER
Experimental Models: Organisms/Strains		
Drosophila:		
ISC/EB driver: *yw;esg-Gal4NP5130,UAS-GFP, UAS-GFPnLacZ/Cyo;tub-Gal80ts/Tm6B*	S. Hayashi; (Goto and Hayashi, 1999)	N/A
EB driver: *Su(H) GBE-gal4, UAS-CD8GFP/Cyo*	S. Hou; (Zeng et al., 2010)	N/A
ISC driver: *esg-gal4, UAS-2XEYFP; Su(H)GBE-gal80, tub-gal80ts/SM5-TM6*	S. Hou; (Wang et al., 2014)	N/A
ISC/EB Flipout system: *w;esg-gal4,tub-gal80ts, UAS-GFP; UAS-flp, Act > CD2 > gal4, UAS-gfp/TM6B*	B. Edgar; (Jiang et al., 2009)	N/A
RalA reporter: *pg89,FRT19A/FM7a;Sp/Cyo*	C. Ghighlione; (Bourbon et al., 2002)	N/A
en-gal4 driver: *y1 w*; P{w+mW.hs = en2.4-GAL4}e16E*	Bloomington *Drosophila* Stock Center (BDSC)	RRID:BDSC_30564
RalBP1-RNAi: *P{KK101635}VIE-260B*	Vienna *Drosophila* Resource Center (VDRC)	105976; RRID:FlyBase_FBst0477802
RalA-RNAi(1): *P{KK108989}VIE-260B*	VDRC	105296; RRID:FlyBase_FBst0477124
RalA-RNAi(2): *y1 v1; P{y+t7.7 v+t1.8 = TRiP.JF03259}attP2*	BDSC	RRID:BDSC_29580
RalA-RNAi(3): *w1118; P{GD8562}v43622*	VDRC	43622; RRID:FlyBase_FBst0465168
Wg-RNAi: *P{KK108857}VIE-260B*	VDRC	104579; RRID:FlyBase_FBst0476437
UAS-Wg: *w*; P{w+mC = UAS-wg.H.T:HA1}6C*	BDSC	RRID:BDSC_5918
UAS-RalAwt(1): *P{UAS-RalA}3*	G. Hasan; (Richhariya et al., 2017)	N/A
UAS-RalAwt(2): *P{UAS-RalA}2*	G. Hasan; (Richhariya et al., 2017)	N/A
UAS-GFP y1 w; P{w+mC = UAS-mCD8::GFP.L}LL5, P{UAS-mCD8::GFP.L}2*	BDSC	RRID:BDSC_5137
UAS-RFP w[1118]; P{w[+mC] = UAS-RedStinger}4/CyO	BDSC	RRID:BDSC_8546
Control genotype *w1118*	R. Cagan	N/A
Apc$^{-/-}$w-;APC1q8,FRT82B/TM6B	Y. Ahmed; (Ahmed et al., 1998)	N/A
MARCM Control *w-; FRT82B, con lacZ*	R. Cagan	N/A
MARCM82B y,w,hsFLP,tub-gal4, UAS-GFP-myc; FRT82B,tub-gal80 CD2+ y+/Tm6B	N. Tapon	N/A
Fz3-RFP	Y. Ahmed; (Olson et al., 2011)	N/A
Delta::GFP reporter *y1 w*; Mi{PT-GFSTF.1} DlMI04868-GFSTF.1/TM6C, Sb1 Tb1*	BDSC	RRID:BDSC_59819
Su(H)GBE-LacZ reporter *w; Sp/CyO; cn ry Su(H)GBE ry+/(TM6B)*	C. Micchelli; (Furriols and Bray, 2001)	N/A
Mouse lines:		
Rala$^{tm1.1Cjm}$/Rala$^{tm1.1Cjm}$	PMID:23063435	RRID:MGI:5505291
Ralb$^{tm1.1Cjm}$/Ralb$^{tm1.1Cjm}$	PMID:23063435	RRID:MGI:5505291
Apc^{tm1Tno}/Apc^{tm1Tno}	PMID:20084116	RRID:MGI:4429571
VilCreER	(el Marjou et al., 2004)	N/A
Lgr5-EGFP-Cre^{ER}	(Barker et al., 2007)	N/A
R26-LoxStopLox-tdTomato	(Madisen et al., 2010),	N/A
RNAscope probes:		
Mm-Axin2 2.5 LS	Advanced Cell Diagnostics, Hayward, CA	Product code: 400338
Mm-Lgr5 2.5 LS Probe	Advanced Cell Diagnostics, Hayward, CA	Product code: 312178
Mm-OLFM4 2.5 LS Probe	Advanced Cell Diagnostics, Hayward, CA	Product code: 311838
Mm-Smoc2 2.5 LS Probe	Advanced Cell Diagnostics, Hayward, CA	Product code: 318548
Mm-RalB-E2 2.5 LS Probe	Advanced Cell Diagnostics, Hayward, CA	Product code: 469688
MM-PPIB 2.5 LS Probe Positive Control	Advanced Cell Diagnostics, Hayward, CA	Product code: 313918

(*Continued on next page*)

Continued		
REAGENT or RESOURCE	SOURCE	IDENTIFIER
Recombinant DNA		
M50 Super 8x TOPFlash	PMID:12699626	RRID:Addgene_12456
pSAR-MT-beta-gal	PMID:8755583	RRID:Addgene_16486
SNAP-Fzd5	(Koo et al., 2012)	N/A
SNAP-Fzd7	Gift from Bienz lab	N/A
Software and Algorithms		
Fiji	NIH	1.51n; https://fiji.sc/
ImageJ	https://imagej.net/Welcome	RRID:SCR_002074
GraphPad Prism 6	GraphPad	RRID:SCR_002798
ZEN 2 lite	Zeiss	RRID:SCR_013672
7500 Real-Time PCR Software	Applied Biosystems	RRID:SCR_014596
BatchQuantify	This paper	https://github.com/emLtwc/2018-Cell-Stem-Cell
Other		
LSM780 microscope	Zeiss	N/A
BX51 microscope	Olympus	N/A
7500 Fast Real-Time PCR System	Applied Biosystems	N/A
AutostainerLink 48	Dako	N/A
Bond Rx autostainer	Leica	N/A
FACSARIA FUSION	BD Biosciences	N/A
Odyssey Clx	LI-COR	N/A
Attune NxT flow cytometer	ThermoFisher Scientific	N/A

CONTACT FOR REAGENT AND RESOURCE SHARING

Requests for further information, reagents, and resources should be directed to and will be fulfilled by the Lead Contact, Owen J. Sansom (o.sansom@beatson.gla.ac.uk).

EXPERIMENTAL MODEL AND SUBJECT DETAILS

Experimental Animals

Species used: *Drosophila melanogaster*, *Mus musculus*

Drosophila breeding and maintenance

Flies were bred and maintained on standard food in humidity and temperature-controlled incubators in a 12h-12h light-dark cycle. Crosses for adult specific transgene manipulations were kept at 18°C. F1s of the desired genotype were collected following 2-3 days of adult eclosion. Animals with temperature sensitive transgenes were switched to 29°C and aged for the time needed to allow transgene activation. *Apc* full mutant animals were always maintained at 18°C. Otherwise, animals were aged at 25°C. Adult posterior midguts, and wing discs of late L3 larvae were analyzed. Standard food used: 10 g Agar, 15 g Sucrose, 30 g Glucose, 15 g Maize meal, 10 g wheat germ, 30 g treacle and 10 g Soya flour per liter of distilled water.

Sex

Only mated females were used for experiments on the *Drosophila* midgut.

Full *Drosophila* genotypes

Full fly genotypes as they appear in each Figure panel are listed in Table S1.

Mouse colonies

All experiments were performed according to UK Home Office regulations (Project License 70/8646), adhered to ARRIVE guidelines and were subject to review by the animal welfare and ethical review board of the University of Glasgow. Standard diet and water was given *ad libitum*, and under non-barrier conditions. The Mice strains used are indicated in the resource table. The Porcupine inhibitor WNT974(LGKT974) was administered in a concentration of 5mg/kg BID (oral) in a vehicle of 0.5% Tween-80/0.5% Methylcellulose. Tamoxifen (Sigma) IP was used to induce VilCreER and Lgr5CreER mice at the indicated concentrations. For regeneration

experiments, mice were exposed to γ-irradiation from caesium-137 sources. This delivered γ-irradiation at 0.423 Gy min−1. Mice were sampled 3 days following irradiation damage. The smallest sample size was used that would still give a significant difference in accordance with the 3Rs. No distinction between males and females has been made in all mice experiments. All mice were above 20 g of weight before eligible participate in any experiment. All mice experiments were performed on a C57BL/6 (n = 5 or more), except from clonal expansion experiments which were perform on mixed background.

METHOD DETAILS

Immunofluorescence of *Drosophila* tissues

Tissues were dissected and fixed in 4% para-formaldehyde (Polysciences, Inc.) at room temperature for a minimum of 30 min. After fixation, tissues were washed 3 times in PBS + 0.2% Triton X-100 (PBST) for 20 min, followed by overnight incubation at 4°C with primary antibodies in PBST + 0.5% Bovine Serum Albumin (BSA) (PBT). Samples were then washed in PBST 3 × 20 minutes and incubated with secondary antibodies in PBT for 3h at room temperature, followed by washing and mounting.

Midguts stained for Wg were fixed in PEM-FA (0.1 M PIPES, 2mM EGTA, 1.0 mM MgSO4, 4% formaldehyde, pH 7.0). Tissues were washed in PBST and blocked in 5% normal goat serum (Sigma) in PBS for 2 hours at room temperature. Following the blocking step samples were subjected to the standard staining protocol described above. For detection of extracellular Wg, wing discs were dissected in PBS and moved to antibody for 1h at room temperature prior to fixation and subsequent processing following standard staining protocol. All samples were mounted onto glass slides (VWR) with 13mm x 0.12mm spacers (Electron Microscopy Science) and Vectashield mounting media containing DAPI (Vector Laboratories, Inc). Confocal images were obtained on a Zeiss LSM 780 and processed in the Zeiss ZEN software.

Antibody concentrations used: anti-Arm (1:10), anti-β-Gal (1:1000), anti-DsRed (1:500), anti-GFP (1:2000), anti-Myc (1:100), anti-Pros (1:20), anti-pH3S10 (1:100), anti-Senseless (1:2000), anti-Wg (1:10 or 1:3 for extracellular staining). Secondary antibodies were used as follows: anti-IgG-488 (1:200), anti-IgG-594 (1:100), IgG-647 (1:50).

Drosophila midgut regeneration assay

Regeneration assays was performed according to (Neyen et al., 2014). Oral infection was induced using *Erwinia carotovora subsp. carotovora 15* (*Ecc15*) (Basset et al., 2000). Bacteria were grown overnight in LB medium in orbital shaker incubator at 30°C, 200 rpm. The bacterial culture was pelleted (Beckman Coulter JS-4.2 rotor, 10 min @3000rpm ≈ 22547 k-factor) and adjusted to OD600 = 200 followed by mixing with a 5% sucrose solution 1:1. Flies used for regeneration experiments were starved for 2 hours prior to infection to synchronize feeding. Animals were moved into vials containing filter paper (Whatman) soaked into 5% sucrose solution (Mock) or the prepared bacterial solution. Flies were dissected 12-16 hours after infection.

Quantification of pH3 positive cells in the *Drosophila* posterior midgut

We used antibodies against phosphorylated Histone 3 to visualize ISC proliferation in the posterior midgut, which is defined as the region between the copper cell region and the hindgut. Number of midguts analyzed (N) for each experiment are indicated in the Figures.

Drosophila MARCM and Flip-out clone analysis

Recombinant clones were generated using the MARCM system (Lee and Luo, 1999) or the temperature-sensitive *esg flip-out* (*esg* $^{F/O}$) system (Jiang et al., 2009). MARCM adults of the desired genotype were subjected to three, 30-minute 37°C heat-shocks separated by 1h at room temperature. Animals were aged for ten or thirty days at 25°C for MARCM and 29°C for flip-out flies. Clonal size in MARCM or *esg*$^{F/O}$ experiments was determined by counting the number of nuclei labeled by DAPI on an Olympus BX51 epi-fluorescent microscope. Clone size was not determined for 30-day old *esg*$^{F/O}$ animals as no distinct clones cloud be identified.

Drosophila RNA extraction and RT-qPCR

Total RNA from a minimum of 15 midguts was extracted using QIAGEN RNAeasy kit, following manufacturer's instructions. RNA was quantified using a NanoDrop 2000c Spectrophotometer.

cDNA was synthesized using the High-Capacity cDNA reverse transcription kit. Quanta SYBR green Master Mix (Low ROX, Fermentas) was used following manufacturer's instructions. Data were obtained and analyzed using the Applied Biosystems 7500 software. Results represent biological triplicates ± SEM. Expression of target genes was measured and normalized to *rpl32.*

Sorting of *Drosophila* ISCs and gene expression assessment

For sorting of ISCs we dissected 100 posterior midguts (R4 + R5). Sample preparation, cell sorting, RNA extraction and RNA amplification were carried out as described by (Dutta et al., 2015) with a minor modification: MessageBOOSTER cDNA Synthesis Kit (Lucigen, Cat No. MB060124) was used to amplify RNA. To eliminate potential bias during RNA amplification, we included 500 pg of RNA from whole posterior midguts, which was subject to the same amplification procedure as the RNA obtained from sorted cells. Gene expression levels from sorted cells where first normalized against the *Rpl32* levels in the same sample, and then presented as a ratio over gene expression in whole posterior midguts. Results represent biological triplicates ± SEM. Primers used for RT-qPCRs are detailed in Table S2.

Drosophila staining quantifications

Fz3-RFP and intestinal Wg was quantified as the average staining intensity within the GFP positive compartment; nuclear dMyc staining was quantified as the average staining intensity within the compartment positive for both DAPI and GFP, normalized by background intensity using a custom ImageJ macro, BatchQuantify. Extracellular Wg staining was analyzed in ZEN 2 (Zeiss).

Immunohistochemistry and RNA *in situ* hybridization

All IHC, special stains and *in situ* hyrbidisation staining was performed on 4um formalin fixed paraffin embedded sections that had previously been heated at 60°C for 2 hours.

The following antibodies were used on a Dako AutostainerLink 48, Brdu (BD Biosciences, UK), CD44 (Cell Signaling, UK), and RFP (Tebu-bio, UK). The tissue sections underwent manual dewaxing through xylene, graded alcohol and then washed in tap water before undergoing heat induced epitope retrieval (HIER). HIER was performed on a Dako PT module where the 4um sections were heated to 98°C for 25 minutes in appropriate retrieval beffer. Sections were placed in PT module buffer 1 (Thermo, UK). After epitope retrieval sections were rinsed in Tris Buffered saline with Tween (Tbt) prior to being loaded onto the autostainer. The sections then underwent peroxidase blocking (Agilent, UK), washed in Tbt before application of primary antibody at a previously optimized dilution (Brdu 1/150; CD44 1/250; RFP 1/150) for 40 minutes. The sections were then washed in Tbt before application of appropriate EnVision (Agilent, UK) secondary antibody dependent on species of primary antibody for 30 minutes. Sections were rinsed in Tbt before applying Liquid DAB (Agilent, UK). The sections were then washed in water, counterstained with hematoxylin and coverslipped using DPX mountant (CellPath, UK).

Caspase 3 (Cell Signaling, UK) and Lysozyme (Agilent, UK) were stained on the Leica Bond Rx autostainer. Sections were loaded onto the autostainer and underwent dewaxing and epitope retrieval on board. Caspase 3 was retrieved using ER2 buffer (Leica, UK) for 30 minutes at 95°C and Lysozyme with Enzyme 1 (Leica, UK) for 5 minutes. The sections were then stained using an Intense R kit (Leica UK). Caspase 3 was diluted 1/500 and Lysozyme 1/300.

Rala, Notch-1, and β-catenin sections were stained manually. These sections underwent manual dewaxing through xylene, graded alcohol and then washed in tap water before undergoing antigen retrieval. Rala sections were boiled 30 min in citric acid buffer, Notch-1 sections 30 min in Protaqs IX buffer (BioCyc), and β-catenin sections 50 min in Tris-EDTA. Rala primary antibody (1:500) was incubated overnight at +4C. Notch-1 antibody (1:50) at 1h RT, and β-Catenin 2h RT.

Sections were stained with Alcian Blue and a PAS stain. These sections underwent manual dewaxing through xylene, graded alcohol and then washed in tap water before undergoing appropriate standard staining protocol for each stain.

In situ-hybridization detection for *Axin2, Ascl2, Lgr5, Olfm4, Ralb-E2,* and *Ppib* (Advanced Cell Diagnostics, Hayward, CA) mRNA was performed using RNAscope 2.5 LS (Brown) detection kit (Advanced Cell Diagnostics, Hayward, CA) on a Leica Bond Rx autostainer strictly adhering to the manufacturer's instructions.

ImageJ was used to quantify detected RNA on images taken at 40X. First the image was duplicated into two. The intestinal crypts were encircled manually in the original image, and added to the ROI manager. The Channels was then split into red, green, and blue. The blue channel was used to put a threshold to only mark the dots in each encircled crypt, and this setting was kept throughout the analysis for all images stained with a specific probe. The percentage of positive area within each crypt was then measured. For each sample at least 25 crypts have been measured, and the average represents one biological sample.

To false color the dots red, the image was first duplicated, and the channels split into red, green, and blue in one of them. The threshold was set in the blue image, and a selection created. This selection was added to the ROI manager, and used in the original image to mark the dots. Once marked, the dots were colored by the fill function. For presentation constrast have been increased to visualize the faint crypt structures obtain by counterstaining.

Crypt and cell culture

The proximal mouse small intestines were washed with PBS and open longitudinal, and cut to small pieces, that were washed in PBS repentantly until the PBS buffer is transparent and free from debris. Further the small pieces containing intestinal crypts were incubated in PBS containing 2mM EDTA during 30min in +4C. 10mL PBS is added and mechanically pipetted up and down to generate a first fraction containing intestinal crypts. This step was repeated and fraction 2-4 collected and filtered through a 70-um cell strainer. Isolated crypts then were mixed with 50 μL of Matrigel (BD Bioscence), plated in 24-well plates in Advanced DMEM/F12 with Noggin (100 ng mL−1, Peprotech). Wild-type crypts were also supplemented with R-spondin (500 ng mL−1; R&D Systems). Growth medium is replaced every other day.

For colony forming experiments, organoids were split into single cells by incubation in Tryple express (GIBCO) supplemented with Dnase (100U) for 30-45 minutes in a 37C water bath, and resuspended mechanically using a pipette every 15 minutes to disperse the cells. 5000 cells were seeded into 10ul Matrigel to allow colony formation over time.

Mycoplasma negative HEK293T cells were grown in DMEM medium supplemented with 10% FCS, 1% Glutamine, 1% Pest, and 1% HEPES. A Plamsid CRISPR-Cas9 containing gRNA was produced according to the manufacturer's instructions (Invitrogen), and YFP positive clones were FACS sorted using the BD FACSARIA FUSION (BD Biosciences) 48h after transfection. All transfection experiments, including SNAP-tag Frizzled-5 and Frizzled-7 were performed using lipofectamine 2000 according to standard protocol (Invitrogen). gRNA oligonucleotides are detailed in Table S2.

For the TopFlash assay cells were transfected with SuperTopflash (Addgene), and B-gal (Addgene) plasmids in a ratio 10:1 using lipofectamine 2000 according to standard protocol. The Dual-Light Luciferase & β-Galactosidase Reporter Gene Assay System

(Thermo Scientific) was used to determine luciferase and b-gal expression. Samples loaded onto clear white bottom 96-well plates were read on a Veritas microplate luminometer (Turner BioSystems).

Cell surface pulldown and western blotting

Confluent cells grown on poly-d-lysine (Sigma-Aldrich) coated 10cm plates were labeled with 0.13 mg/mL sulfo-NHS-SS- biotin in PBS, during 1h on rocking table in +4C, after two washes of PBS cells were scraped off and sonicated in 500 μL PBS (supplemented with protease inhibitors). To 450ul 50ul of streptavidin coated beads (New England Biolabs inc.) was added, and 50 μL was analyzed as whole cell lysate. Beads and protein suspension was incubated retaining in +4C overnight, to be analyzed with western blot.

Nuclear fraction was isolated and protein concentrations were determined using a BCA Protein Assay Kit (Pierce). Equal amounts of cellular protein (30 μg) were separated on a 4%–12% gradient gel (Novex) and subsequently transferred to a PVDF membrane (Amersham). Total protein was visualized with Poinceau (Sigma). After blocking the membranes in TBS containing 5% BSA (Sigma), 0.02% Triton X-100 for 1 h, primary antibodies were added: After washing, the appropriate DyLight 800 or 580 fluorescently-conjugated secondary goat antibodies (Thermo Scientific, 1:10 000) were added in block solution for 1 h in room temperature on a rocking table. Antibody binding was detected using the Li-COR Odyssey CLx. Primary antibody (see resource table) incubations were carried out at 4°C overnight. All primary antibodies (resource table) were used (1:1000) for WB applications.

Internalization assays

Mycoplasma free HEK293T Cells were transfected with SNAP-tagged Frizzled constructs, and 24h later plated onto poly-d-lysine (Sigma-Aldrich) coated coverslips in 24-wells. After additional 24h incubation, cells were washed once with PBS, and incubated with diluted SNAP-Vista® Green 1:1000 (New England Biolabs inc.) in PBS for 5 minutes in room temperature. To follow internalization, standard DMEM medium containing 10% serum was added to cells and incubated according to indicated time points. Cells were fixed in 4% PFA and internalization was analyzed using a Zeiss 710 confocal microscope.

For internalization assay of endogenous protein cells were grown on poly-d-lysine (Sigma-Aldrich) coated 10 cm plates until confluent, and incubated in +4C during 1h in 0.13 mg/mL sulfo-NHS-SS- biotin (Sigma-Aldrich) in PBS. Cells were washed twice in cold PBS, and cell culture medium was added to plates, and then incubated for 2.5, 5, or 10 minutes in 37C in cell culture media as indicated. After incubation cells were washed 1h in 4C in 15/mg/mL MesNA(Sigma-Aldrich) diluted in PBS and supplemented with 10mM NaOH. To inactivate the MesNA 1mL of IAA (Sigma-Aldrich) in PBS was added to each sample and incubated 15min in 4C. After two PBS washes samples were lysed in RIPA buffer.

For detection ELISA plates (Thermo Scientific) were coated with primary antibody for 4h in RT, and blocked 1h in BSA-block. After two washes in TBST samples were added to the plates and incubated overnight in +4C. Next, Plates were washed twice and streptavidin-conjugated horseradish (1:1000) was added onto the plate. After two washes in TBST and two washes in PBS signal was detecting using SuperSignal Elisa Pico (ThermoFisher Science) on a Spark microplate reader (Tecan).

qPCR

For mice samples approximately 1cm from the proximal small intestine was first isolated and stored in RNAlater. A small piece of the samples were further placed in vials containing CK14 ceramic beads and RLT buffer (QIAGEN RNAeasy kit) supplemented with β-mercaptoethanol. Samples were lysed using a Precellys machine. RNA was afterward extracted from lysed samples using the QIAGEN RNAeasy kit, following manufacturer's instructions.

Further, cDNA was generated from mice RNA using Quantitect Reverse Transcription Kit (QIAGEN) in a reaction volume of 20 μl. qPCR reactions were prepared (15 μl), of 7.5 μL of 2 × DyNAmo HS master mix (Thermo Scientific), 0.5 μM reverse and forward primers, and 1.5 μL cDNA. The qPCR was preformed according to manufactures protocol. Gapdh was used to normalize for differences in RNA input. Primers used for RT-qPCRs are detailed in Table S2.

Clonal analysis in mice

Lgr5CreER tdTom^{fl} mice were induced with 0.15mg tamoxifen (IP) as previously described (Snippert et al., 2014). The small intestines of mice were sampled at different time points and fixed with freshly prepared 4% paraformaldehyde (PFA) for 3 hours at room temperature. The small intestinal tissue was then incubated with DAPI (10ug/mL) in 0.1% PBS-Tween20 (PBS-T) over night. Whole mount sections were imaged using a Zeiss 710 confocal microscope.

FACS

Organoids were split into single cells by incubation in Tryple express (GIBCO) supplemented with Dnase (100U) for 30-45 minutes in a 37C water bath, and resuspended mechanically using a pipette every 15 minutes to disperse the cells. Single cells were isolated using a 40-um cell strainer, washed twice in PBS, and blocked for 30 min in PBS/BSA in RT. Frizzled-7 antibody (1:500) labeled with Alexa Fluor fluorochrome (ThermoFisher Scientific) was incubated in blocking medium during 15 min RT. Cell surface levels of Frizzled-7 on living cells were measured on the Attune NxT flow cytometer (ThermoFisher Scientific), and DAPI incorporation was used as a dead/live markers.

Statistical analysis

Graph Pad Prism 6 software was used for statistical analyses. Information on sample size, biological replicas, independent samples, independent experiments, and statistical tests used for each experiment are indicated in the figure legends.

DATA AND SOFTWARE AVAILABILITY

The custom ImageJ macro, BatchQuantify, used for *Drosophila* immunofluorescent staining quantification is available at https://github.com/emLtwc/2018-Cell-Stem-Cell.